Department of Radio Science and Engineering

Characterization, modeling, and design for applications of waveguide impedance tuners and Schottky diodes at millimeter wavelengths

Tero Kiuru

Aalto University

DOCTORAL DISSERTATIONS

Aalto University publication series
DOCTORAL DISSERTATIONS 133/2011

Characterization, modeling, and design for applications of waveguide impedance tuners and Schottky diodes at millimeter wavelengths

Tero Kiuru

Doctoral dissertation for the degree of Doctor of Science in Technology to be presented with due permission of the School of Electrical Engineering for public examination and debate in Auditorium S1 at the Aalto University School of Electrical Engineering (Espoo, Finland) on the 12th of December 2011 at 13:00 o'clock.

Aalto University
School of Electrical Engineering
Department of Radio Science and Engineering

Supervisor
Professor Antti Räisänen

Instructors
Dr. Juha Mallat, Aalto University, Espoo, Finland
Dr. Tapani Närhi, European Space Agency, Noordwijk, The Netherlands

Preliminary examiners
Dr. Thomas Crowe, Virginia Diodes Inc., Charlottesville, VA, USA
Dr. Imran Mehdi, Jet Propulsion Laboratory, Pasadena, CA, USA

Opponent
Professor Jan Stake, Chalmers University of Technology, Göteborg, Sweden

Aalto University publication series
DOCTORAL DISSERTATIONS 133/2011

© Tero Kiuru

ISBN 978-952-60-4408-8 (pdf)
ISBN 978-952-60-4407-1 (printed)
ISSN-L 1799-4934
ISSN 1799-4942 (pdf)
ISSN 1799-4934 (printed)

Unigrafia Oy
Helsinki 2011

Finland

The dissertation can be read at http://lib.tkk.fi/Diss/

Aalto University

Aalto University, P.O. Box 11000, FI-00076 Aalto www.aalto.fi

Abstract

Author
Tero Kiuru

Name of the doctoral dissertation
Characterization, modeling, and design for applications of waveguide impedance tuners and Schottky diodes at millimeter wavelengths

Publisher School of Electrical Engineering

Unit Department of Radio Science and Engineering

Series Aalto University publication series DOCTORAL DISSERTATIONS 133/2011

Field of research Radio engineering

Manuscript submitted 29 August 2011 **Manuscript revised** 8 November 2011

Date of the defence 12 December 2011 **Language** English

☐ **Monograph** ☒ **Article dissertation (summary + original articles)**

Abstract

This work contributes to two fields of research at millimeter wavelengths: waveguide impedance tuners and Schottky diodes. Three novel impedance tuning devices for frequencies between 75-220 GHz are presented and new modeling and characterization methods applicable to millimeter-wave and THz Schottky diodes are introduced. In addition, the use of waveguide impedance tuners and Schottky diodes is demonstrated in three different applications. Waveguide tuners are used for dielectric material characterization at 75-110 GHz and in a fundamental frequency mixer diode test platform at 183 GHz. Schottky diodes characterized in this work are used in a novel MMIC frequency tripler for 75-140 GHz and in the aforementioned 183 GHz mixer diode test platform.

Waveguide impedance tuners are widely used in a variety of applications at millimeter wavelengths, ranging from device matching to load-pull and noise parameter measurements. The three impedance tuners presented in this work are a multiwaveguide-band backshort, waveguide EH-tuner for 140-220 GHz, and a double-stub E-plane tuner for 75-110 GHz. All impedance tuners are based on the dielectric backshort concept, which offers resonance-free operation, low losses, and tuning with higher resolution than is possible with traditional backshorts. For example, at the center frequency of the W-band, 92 GHz, the VSWR of the multiwaveguide-band backshort is larger than 165 for all positions of the backshort and the phase resolution as a function of the backshort movement is 0.0825 (deg)/10 micrometers, which is 10 times more accurate than with a traditional backshort.

The Schottky diode is the workhorse in almost all room temperature mixer and frequency multiplier applications at 100-3000 GHz. Design of Schottky-based circuits at these frequencies relies on accurate models for the Schottky diode. In this work, a novel method is presented for simultaneous extraction of Schottky diode series resistance and thermal resistance. The method avoids the inaccuracies inherent in the traditional I-V extraction methods caused by the self-heating of the diode, which can result in too small a value for the extracted series resistance. In addition, a quantitative comparison of low-frequency (1 MHz) and microwave frequency (3-10 GHz) capacitance determination techniques is performed for millimeter-wave and THz Schottky diodes.

Keywords Waveguide impedance tuner, Schottky diode, mixer, frequency multiplier

ISBN (printed) 978-952-60-4407-1 **ISBN (pdf)** 978-952-60-4408-8

ISSN-L 1799-4934 **ISSN (printed)** 1799-4934 **ISSN (pdf)** 1799-4942

Location of publisher Espoo **Location of printing** Helsinki **Year** 2011

Pages 91 **The dissertation can be read at** http://lib.tkk.fi/Diss/

Aalto-yliopisto

Tiivistelmä

Aalto-yliopisto, PL 11000, 00076 Aalto www.aalto.fi

Tekijä
Tero Kiuru

Väitöskirjan nimi
Karakterisointi, mallinnus ja suunnittelu aaltoputki-impedanssisäädinten ja Schottky-diodien sovelluksiin millimetriaaltoalueella

Julkaisija Sähkötekniikan korkeakoulu

Yksikkö Radiotieteen ja -tekniikan laitos

Sarja Aalto University publication series DOCTORAL DISSERTATIONS 133/2011

Tutkimusala Radiotekniikka

Käsikirjoituksen pvm 29.08.2011 **Korjatun käsikirjoituksen pvm** 08.11.2011

Väitöspäivä 12.12.2011 **Kieli** Englanti

☐ **Monografia** ☒ **Yhdistelmäväitöskirja (yhteenveto-osa + erillisartikkelit)**

Tiivistelmä
Tämä työ käsittelee kahta millimetriaaltoalueen tutkimusalaa: aaltoputki-impedanssisäätimiä ja Schottky-diodeja. Työssä esitellään kolme uudentyyppistä impedanssinsäätölaitetta taajuusalueelle 75-220 GHz sekä uusia mallinnus- ja karakterisointimenetelmiä millimetriaalto- ja terahertsialueen Schottky-diodeille. Lisäksi kolme työssä suunniteltua laitetta havainnollistaa aaltoputki-impedanssisäädinten ja Schottky-diodien käyttöä eri sovellusalueilla. Aaltoputki-impedanssisäätimiä käytetään työssä dielektrisen materiaalin mittaamiseen 75-110 GHz:n taajuusalueella sekä sekoitindiodien testialustassa 183 GHz:n taajuudella. Työssä karakterisoituja Schottky-diodeja käytetään uudenlaisessa monoliittisessa taajuuskolmentajassa 75-140 GHz:n taajuusalueella sekä edellä mainitussa testialustassa.

Aaltoputki-impedanssisäätimiä käytetään millimetriaaltoalueella useissa sovelluksissa esimerkiksi laitteiden impedanssin sovittamiseen, load-pull -mittauksiin sekä kohinaparametrimittauksiin. Kolme työssä esiteltyä impedanssin säätölaitetta ovat moniin erikokoisiin aaltoputkiin soveltuva oikosulku, aaltoputki-EH-impedanssisäädin 140-220 GHz:n taajuusalueelle sekä E-tason kaksoisvirityspätkäsäädin 75-110 GHz:n taajuuksille. Kaikki impedanssisäätimet hyödyntävät ns. dielektrisen oikosulun ideaa, joka mahdollistaa resonanssivapaan ja vähähäviöisen toiminnan sekä paremman säätötarkkuuden kuin perinteiset aaltoputkioikosulut. Esimerkiksi W-kaistan keskitaajuudella, 92 GHz:llä, kehitetyn erikokoisiin aaltoputkiin soveltuvan oikosulun SAS on suurempi kuin 165 kaikilla oikosulun asennoilla ja vaiheresoluutio oikosulun liikkeen funktiona 0,0825 (astetta)/10 mikrometriä, joka on 10 kertaa tarkempi kuin perinteisillä oikosuluilla.

Schottky-diodi on käytetyin elementti 100-3000 GHz:n taajuusalueella huoneenlämmössä toimivissa sekoitin- ja taajuuskertojasovelluksissa. Schottky-diodeihin perustuvien piirien suunnittelu on tarkkojen Schottky-diodimallien varassa. Työssä esitellään uusi menetelmä, jolla on mahdollista määrittää samanaikaisesti Schottky-diodien sarjavastuksen arvo sekä arvio lämpöresistanssille. Uusi menetelmä välttää diodin itsensä kuumenemisesta johtuvat epätarkkuudet perinteisissä virta-jännite -parametrien määritysmenetelmissä, joiden vuoksi määritetty sarjaresistanssi on pienempi kuin todellinen sarjaresistanssi. Lisäksi kvantitatiivinen matalan taajuuden (1 MHz) ja mikroaaltotaajuuden (3-10 GHz) kapasitanssin määritystekniikoiden vertailu on suoritettu millimetriaalto- ja terahertsialueen Schottky-diodeille.

Avainsanat Aaltoputki-impedanssisäädin, Schottky-diodi, sekoitin, taajuuskertoja

ISBN (painettu) 978-952-60-4407-1 **ISBN (pdf)** 978-952-60-4408-8

ISSN-L 1799-4934 **ISSN (painettu)** 1799-4934 **ISSN (pdf)** 1799-4942

Julkaisupaikka Espoo **Painopaikka** Helsinki **Vuosi** 2011

Sivumäärä 91 **Luettavissa verkossa osoitteessa** http://lib.tkk.fi/Diss/

Preface

This doctoral thesis has been carried out at the Department of Radio Science and Engineering (former Radio Laboratory) at Aalto University, School of Electrical Engineering during 2006-2011. In 2007-2010 I participated in the European Space Agency's Networking/Partnering Initiative program which included a one-year working visit to the European Space Research and Technology Centre (ESTEC) in 2008.

My warmest gratitude goes to my supervisor, Professor Antti Räisänen, for his guidance and support during this research. I also highly appreciate the in-depth expertise of my instructors, Dr. Juha Mallat and Dr. Tapani Närhi and their ability and willingness to share that expertise with me. Dr. Ville Möttönen and Ms. Krista Dahlberg deserve warm thanks for their contributions to the work in this thesis.

Special thanks go to a large group of colleagues working with ESTEC and with several ESA projects for sharing valuable advice and for helping me to see the bigger picture. Thank you Petri, Ville, Anttu, Oleg, Byron, Tomasz, Eric, John, Dimitri and others.

I want to thank my friends here at the department, who have contemplated mysteries of radio engineering (and other) with me and making my cubicle not only a place to work but also a place where it is always nice to come in the mornings. Thank you Pekka, Olli, Antti, Jari, Aleksi, Veli-Matti, Dmitry, Azremi, Risto, Eikka and many more.

Thank you mom and dad, my sister Tiina and brother Tapio for always supporting and encouraging me.

Thank you Ninu for your love and support. You and the little "creature" growing in your belly help me to remember what is important in life.

Espoo, August 20, 2011 Tero Kiuru

Contents

Preface 7

Contents 8

List of Publications 10

Author's Contribution 11

List of Abbreviations 13

List of Symbols 15

1 Introduction 18

1.1 Motivation and Scope of the Thesis 19
1.2 Scientific Contributions of the Thesis 20

2 Design Aspects at Millimeter Wavelengths 22

2.1 Effect of the Atmosphere 22
2.2 Impedance Matching 23
2.3 Nonlinear Device Modeling and Characterization 24
2.4 Simulation Tools 25

3 Impedance Tuners 26

3.1 Waveguide Backshorts 27
3.1.1 Multiwaveguide-Band Backshort 29
3.2 Sliding Screw- and Stub-Based Waveguide Impedance Tuners 33
3.2.1 *E*-plane Double-Stub Tuner for the W-Band 34
3.2.2 *EH*-Tuner for the G-band 36
3.3 Short Summary and Discussion on Waveguide Impedance Tuners 39

4 Schottky Diode 41

4.1 Fundamentals of the Schottky Diode..41

4.1.1 Barrier Formation..42

4.1.2 Current-Voltage Characteristics 44

4.1.3 Capacitance-Voltage Characteristics...46

4.1.4 Frequency Conversion...46

4.2 Schottky Diode Modeling...47

4.2.1 Physical Modeling of the Schottky Junction..................................48

4.2.2 Equivalent Circuit Approach 48

4.2.3 Full-Wave Modeling 49

4.2.4 Combined Circuit Simulation and Full-Wave Approach 50

4.3 Schottky Diode Measurements...51

4.4 Schottky Diode Characterization and Parameter Extraction 53

4.4.1 I-V Parameter Extraction...53

4.4.2 C-V Parameter Extraction..56

4.4.3 S-parameter Measurement and Characterization..........................57

4.4.4 Schottky Diode Series and Thermal Resistance Extraction 59

4.4.5 Comparison of Low-Frequency and Microwave Frequency Capacitance Determination Techniques 62

4.5 Short Summary on Schottky Diode Modeling and Characterization Results 66

5 Applications 68

5.1 Material Measurement at the W-Band Using Multiwaveguide-Band Backshort 68

5.2 MMIC Frequency Tripler for 75-140 GHz 71

5.3 Waveguide Mixer Test Jig for 183 GHz 73

6 Conclusions and Future Work 78

References 81

Errata..91

List of Publications

This thesis consists of an overview and the following publications which are referred to in the text by their Roman numerals.

[I] T. Kiuru, V. S. Möttönen, and A. V. Räisänen, ”W-band waveguide impedance tuner utilizing dielectric-based backshorts,” *IEEE Transactions on Microwave Theory and Techniques*, vol. 55, no. 8, pp. 1659-1665, Aug. 2007.

[II] T. Kiuru, K. Dahlberg, J. Mallat, A. V. Räisänen, and T. Närhi, ”Noncontacting multiwaveguide-band backshort for millimeter wave applications,” *IEEE Microwave and Wireless Components Letters*, vol. 20, no. 9, pp. 483-485, Sept. 2010.

[III] T. Kiuru, K. Dahlberg, J. Mallat, A. V. Räisänen, and T. Närhi, ”EH-Impedance tuner with dielectric-based backshorts for millimetre wave diode testing,” *European Microwave Conference*, Paris, France, Sept. 2010, pp. 1357-1360.

[IV] T. Kiuru, K. Dahlberg, J. Mallat, and A. V. Räisänen, ”A method for determining the dielectric constant at millimeter wave frequencies,” *Global Symposium on Millimeter Waves*, Incheon, Korea, April, 2010, pp. 331-334.

[V] T. Kiuru, J. Mallat, A. V. Räisänen, and T. Närhi, ”Schottky diode series resistance and thermal resistance extraction from S-parameter and temperature controlled I-V measurements,” *IEEE Transactions on Microwave Theory and Techniques*, vol. 59, no. 8, pp. 2108-2116, Aug. 2011.

[VI] T. Kiuru, K. Dahlberg, J. Mallat, A. V. Räisänen, and T. Närhi, ”Comparison of low-frequency and microwave frequency capacitance determination techniques for mm-wave Schottky diodes,” *European Microwave Integrated Circuits Conference*, Manchester, UK, Oct. 2011, pp. 53-56.

[VII] T. Kiuru, J. Mallat, A. V. Räisänen, and T. Närhi, ”Compact broadband MMIC Schottky frequency tripler for 75 – 140 GHz,” *European Microwave Integrated Circuits Conference*, Manchester, UK, Oct. 2011, pp. 108-111.

[VIII] K. Dahlberg, T. Kiuru, J. Mallat, A. V. Räisänen, and T. Närhi, ”Generic jig for testing mixing performance of millimeter wave Schottky diodes,” *European Microwave Conference*, Manchester, UK, Oct. 2011, pp. 922-925.

Author's Contribution

[I] This is the result of collaborative work. The impedance tuner was designed by the author together with Dr. Ville Möttönen. The author carried out the simulations, performed the measurements and was responsible for writing the publication. The idea for the waveguide impedance tuner was proposed by Dr. Möttönen. Prof. Antti Räisänen supervised the work.

[II] The work was mainly done by the author. The author proposed the idea for the multiwaveguide-band backshort, carried out the design, simulations and measurements and was responsible for writing the publication. Ms. Krista Dahlberg helped with the simulations. Dr. Juha Mallat, Dr. Tapani Närhi and Prof. Antti Räisänen supervised the work.

[III] The work was mainly done by the author. The idea for the split-waveguide block *EH*-tuner was formulated by the author and Dr. Tapani Närhi. The author carried out the design, simulations and measurements and was responsible for writing the publication. Ms. Krista Dahlberg helped with the simulations and in the mechanical design. Dr. Juha Mallat and Prof. Antti Räisänen supervised the work.

[IV] The work was mainly done by the author. The idea for measuring the dielectric constant using the device presented in [II] was formulated by the author. The author carried out the design, simulations and measurements and was responsible for writing the publication. Ms. Krista Dahlberg helped with the simulations and measurements. Dr. Juha Mallat and Prof. Antti Räisänen supervised the work.

[V] The work was mainly done by the author. The author formulated the idea presented in the paper, developed the numerical method for extracting the series resistance and thermal resistance, and was responsible for writing the publication. The measurements were performed together with Mr. Hannu Hakojärvi. Dr. Juha Mallat and Dr. Tapani Närhi helped in the finalization of the method. Prof. Antti Räisänen supervised the work.

[VI] The work was mainly done by the author. The author formulated the idea for the comparison of different C-V extraction methods, wrote the codes, carried out the simulations and was responsible for writing the publication. The measurements were done together with Ms. Krista Dahlberg and Mr. Hannu Hakojärvi. Ms. Dahlberg also helped with the numerical extraction routines. Dr. Juha Mallat, Dr. Tapani Närhi and Prof. Antti Räisänen supervised the work.

[VII] The work was mainly done by the author. The author designed the device, developed the models for the diodes used in the device, performed the simulations and was responsible for writing the publication. The measurements were performed together with Mr. Hannu Hakojärvi. Dr. Juha Mallat and Dr. Tapani Närhi presented many helpful suggestions during the design. Prof. Antti Räisänen supervised the work.

[VIII] This work was a collaborative effort. The idea was formulated by Ms. Krista Dahlberg, the author, and Dr. Tapani Närhi. Ms. Dahlberg and the author carried out the design with Dr. Juha Mallat. Ms. Dahlberg and the author carried out the simulations and Ms. Dahlberg performed the measurements and assembled the device. Ms. Dahlberg was responsible for writing the publication. The author and Ms. Dahlberg designed the mechanical structure of the device together with Mr. Eino Kahra. Prof. Antti Räisänen supervised the work.

List of Abbreviations

AC	Alternating current
ADS	Advanced Design System
BES	Buried Epitaxial Schottky
CPW	Coplanar waveguide
C-V	Capacitance-voltage
DC	Direct current
DSB	Double-sideband
DUT	Device under test
EHF	Extremely high frequency
FEM	Finite element method
GaAs	Gallium arsenide
GSG	Ground-signal-ground
HB	Harmonic balance
HBV	Heterostructure barrier varactor
HFSS™	High Frequency Structure Simulator
IF	Intermediate frequency
ITU	International Telecommunications Union
I-V	Current-voltage
LO	Local oscillator
MEMS	Microelectromechanical system

MIC	Microwave integrated circuit
MMIC	Monolithic microwave integrated circuit
RF	Radio frequency
SiO_2	Silicon dioxide
SSB	Single-sideband
VSWR	Voltage standing wave ratio
WLAN	Wireless local area network

List of Symbols

a	Waveguide width
A^{**}	Modified Richardson constant
b	Waveguide height
C_{g1}	Pad edge-to-ground capacitance
C_{g2}	Pad edge-to-ground capacitance
C_j	Junction capacitance
C_{jo}	Zero-bias junction capacitance
C_p	Parasitic capacitance
C_T	Total capacitance
E_{oo}	Constant for a given material for a constant doping density
E_F	Fermi level
$E_{F,m}$	Fermi level in metal
$E_{F,s}$	Fermi level in semiconductor
g_j	Small signal junction conductance
h_h	Height of the rectangular hole in the multiwaveguide-band backshort
h_s	Height of the dielectric slab in the multiwaveguide-band backshort
I	Current
I_S	Saturation current
k	Boltzmann's constant
L_{DSB}	Double-sideband conversion loss

L_i	Conversion loss at image frequency
L_{ind}	Finger inductance
L_S	Conversion loss at signal frequency
P_T	Power dissipated in the junction
q	Elementary charge (also electron charge)
$q\Phi_M$	Metal work function
$q\Phi_S$	Semiconductor work function
r_a	Anode radius
r_j	Small signal junction resistance
R_S	Series resistance
R_θ	Thermal (spreading) resistance
S	Surface area of the junction
T_o	Ambient temperature
T_J	Junction temperature
V	Voltage
V_b	Applied voltage (bias voltage)
[1] V_{bi}	Built-in voltage (diffusion voltage)
w_h	Width of the rectangular hole in the multiwaveguide-band backshort
w_s	Width of the dielectric slab in the multiwaveguide-band backshort
Z_o	Characteristic impedance of a transmission line

[1] In this document $V_{bi} = \Phi_{bi}$ = built-in potential. V_{bi} is used throughout Paper [VI] and Φ_{bi} is used elsewhere.

Z_L	Load impedance
$\Delta R_{S,error}$	Error in the extracted value for the series resistance
ΔV_{error}	Error in the junction voltage
ε_o	Permittivity of the vacuum
ε_r	Dielectric constant
ε_s	Permittivity (of semiconductor)
η	Ideality factor
λ_g	Wavelength in waveguide
$\lambda_{g,\ diel}$	Wavelength in waveguide with dielectric slab
ρ	Voltage reflection coefficient
ρ_{dB}	Reflection coefficient in decibel units
ρ_θ	Thermal resistivity
τ	Thermal time constant
φ	Reflection coefficient phase
Φ_B	Schottky barrier voltage
Φ_{bi}	Built-in voltage (diffusion voltage)
χ	Electron affinity

1 Introduction

The millimeter wave region (i.e., millimeter waves) is defined as that part of the electromagnetic spectrum with a wavelength ranging between 10 mm and 1 mm. On the frequency scale, this corresponds to frequencies between 30 GHz and 300 GHz. The International Telecommunications Union (ITU) designates this frequency range as the extremely high frequency (EHF) band. Depending on the source of information, the terahertz (THz) frequency range is often defined as starting from 0.1 THz (100 GHz) and thereby partly overlaps with the millimeter wave region.

From the application point of view, millimeter waves have several advantages over longer electromagnetic waves. These include the possibility of miniaturizing key components, such as antennas, as well as higher data rates in communication. Furthermore, the strong resonances of certain gaseous elements such as oxygen, ozone, and water vapor, are located at millimeter wavelengths, thus enabling the study of atmospheric phenomena using millimeter wave technologies. However, one drawback is the higher atmospheric loss compared to that at lower frequencies, which makes it difficult to utilize millimeter wavelengths in long-range systems inside the atmosphere.

Pioneering research was conducted on the generation and detection of millimeter waves as early as the 1890s. However, it were the military applications during and after World War II that spurred the rapid development of the technology needed for future exploitation of the millimeter wave region. These early applications, of course, worked at microwave frequencies [1]. Military interest in millimeter waves remained strong and was accompanied by applications of space science, radio astronomy, and earth observation in the late 1960s. Subsequently, in the following decades, space applications have become the main driving force for civilian millimeter-wave applications and remain an area of considerable scientific interest. A notable, recent example is the Planck satellite, which uses several extremely sensitive millimeter wave receivers to map the anisotropies in the cosmic microwave background.

Commercial research and development of millimeter wave devices and systems started in the 1970s with the emphasis on the communication technology [2], which benefited vastly from the large bandwidths and available frequencies at millimeter wavelengths.

Today, a number of millimeter wave applications have become commercially available, including, wireless wideband data transmission systems operating at license-free frequencies around 60 GHz, automotive radar systems between 76-81 GHz (applications do not cover the whole band but only certain frequencies inside the band), E-band point-to-point links at 71-76 GHz and at 81-86 GHz, as well as millimeter wave imaging systems at 94 GHz. Above 100 GHz, imaging systems are available at 140 GHz and at 220 GHz and radiometric receivers cover the whole millimeter wave region. Other niche applications exists as well, though the frequencies from 100 GHz to 300 GHz still remain relatively unused commercially.

In the near future, wireless data transmission systems, such as 60 GHz wireless local area networks (WLAN), E-band point-to-point links, as well as automotive radar applications, are expected to penetrate mass markets and bring millimeter wave technology into everyday use. At the same time, the research focus in the commercial sector will shift to ever higher frequencies in order to benefit from the inherent advantages of smaller wavelengths and higher frequencies.

1.1 Motivation and Scope of the Thesis

The development and large-scale implementation of millimeter wave components and systems still faces many challenges. Perhaps the most difficult component of a millimeter wave system is the solid-state source, which should be reliable, high-power, widely tunable, and preferably inexpensive [3]. Due to a lack of such sources (or due to their great expense), the available power at millimeter waves is usually scarce, thus emphasizing the careful design and impedance matching of components. In the design, a particular problem, especially above 100 GHz, is the reduced accuracy of circuit models for passive components and active devices, such as transistors and diodes. Inadequate models may lead to an increase in the number of fabrication runs, thereby raising overall costs.

In this thesis, work has been done to alleviate some of these challenges. Novel impedance matching devices are developed for the waveguide environment and for several waveguide frequency bands. Characterization and modeling methods are

developed, which enable better circuit models for millimeter wave Schottky diodes. In addition, applications are presented that utilize the developed impedance matching devices, Schottky devices, and novel modeling methods.

The thesis is organized as follows. After the Introduction, Chapter 2 discusses general design aspects at millimeter wavelengths. In Chapter 3, three different impedance transforming devices for waveguide environment are presented [I]-[III]. Chapter 4 discusses the Schottky diode and its modeling and characterization aspects [V], [VI]. Chapter 5 presents three applications based on Schottky diodes and/or impedance tuners [IV], [VII], [VIII]. Finally, Conclusions chapter summarizes the performed work. It also concludes the first part of the thesis. The second part of the thesis consists of articles [I]-[VIII] and contains a detailed discussion of the main scientific results of the thesis.

1.2 Scientific Contributions of the Thesis

The scientific merit of the thesis lies in the following novel devices, new methods and improvements in the current state-of-the-art. List items 1 and 2 relate to impedance tuners, 3 to the modeling and characterization of the Schottky devices and 4-6 to applications based on impedance tuners and/or Schottky devices.

1. The first tunable waveguide backshort compatible with several different waveguide sizes

2. Novel waveguide impedance tuners with advantages over traditional waveguide impedance tuners using traditional backshorts, such as high-resolution tuning, no resonance behavior from the backshort structure and relaxed machining tolerances

3. A novel method for the simultaneous determination of Schottky diode thermal resistance and series resistance taking into account the thermal effects from self-biasing

4. The first millimeter wave fully monolithic frequency multiplier to cover two overlapping waveguide frequency bands

5. A millimeter-wave mixer test platform for single anode Schottky diodes with the possibility of changing the diode under test and flexible tuning of RF, LO, and IF impedances

6. A novel method for broadband determination of the dielectric constant of solid materials at millimeter wavelengths using a waveguide backshort

2 Design Aspects at Millimeter Wavelengths

Several aspects should be taken into account when designing components and systems operating at millimeter wavelengths. Important aspects include attenuation of the atmosphere, operation frequency, size limits, available models for active and passive devices, all of which can influence the choices that must be made by the designer in order to achieve the best possible result. This chapter discusses the important physical and technological constraints at millimeter wavelengths, the concept of impedance matching, as well as the modeling and characterization methods and simulation tools used for the work presented in this thesis.

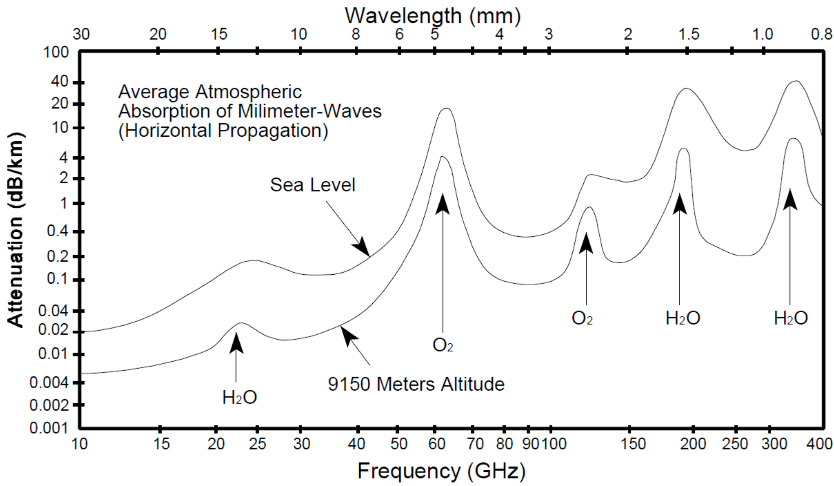

Figure 1. Atmospheric attenuation at millimeter wavelengths [4].

2.1 Effect of the Atmosphere

Atmospheric attenuation increases with increasing frequency and is especially high at the resonance frequencies of oxygen (~60 GHz and ~118 GHz) and water vapor (~183 GHz). Figure 1 shows atmospheric attenuation at sea level and at 9150 m altitude as a function of frequency [4]. The larger attenuation at millimeter wave frequencies compared to that at microwave frequencies is the main reason for the lack of long-range applications in communication and radar systems inside the atmosphere.

However, certain medium-range applications, such as the E-band point-to-point links, can be realized at atmospheric window frequencies, while some short-range applications (e.g., 60 GHz WLAN) actually benefit from greater attenuation, as it enables similar systems to operate at close proximity without interference from each other. In medium-range applications, higher atmospheric loss can be somewhat compensated by the increased gain of millimeter wave antennas compared to that of antennas of the same size at lower frequencies.

2.2 Impedance Matching

Impedance matching or tuning is one of the key topics in radio engineering. Basically all devices and systems working at radio, microwave, or millimeter wave frequencies employ some kind of matching networks. Figure 2 illustrates the impedance matching of a load impedance, Z_L, to a characteristic impedance of the transmission line, Z_o. The load impedance is transformed to the characteristic impedance of the transmission line by the matching circuit and the reflections are cancelled.

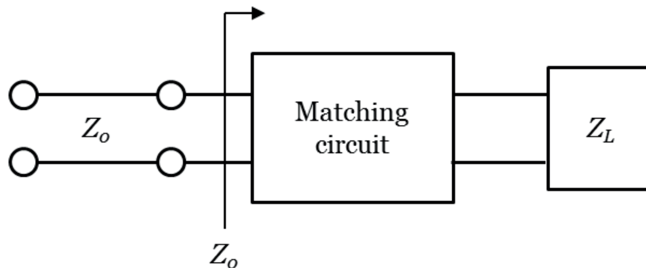

Figure 2. Illustration of impedance matching.

The cancellation of the reflection and providing maximum power to the load is usually the most common reason for impedance matching. However, devices such as amplifiers or mixers are sometimes matched for optimum noise performance and not for optimum gain or conversion loss. In such cases, some reflection from the load is deliberately allowed. In practice, several methods exist for impedance matching in different operating environments [5], [6]. An in-depth discussion of these methods is outside the scope of this work and only stub matching is considered as it is related to

the scientific results of the thesis. A fixed load impedance can be matched using a fixed matching circuit. If the load impedance changes, the matching circuit must change as well. This type of variable matching circuit is referred to as an impedance tuner.

2.3 Nonlinear Device Modeling and Characterization

Nonlinear device modeling is a vast area of research. This section briefly explains the two main philosophies in nonlinear device modeling and positions the modeling work presented in the thesis into this context. These modeling approaches can be roughly divided into physical (i.e., compact) models or measurement-based (i.e., black box) models [7]. Combinations of these models are also possible and very often, as is the case in this work, a complete model for a component or a device consists of both, measurement-based linear and physical nonlinear parts.

The physical models are defined as a set of equations, relating to specific physical properties of the device. The advantages of the physical models are that they can be used to optimize the device in the fabrication phase and that they can account for any combination of input parameters, such as temperature and voltage, or even material parameters like doping density or dielectric constant. The drawback is that finding the correct equations (if they exist) might prove to be extremely difficult. Moreover, extraction of the parameters for the equations may not be straightforward, e.g., if the equivalent circuit is complex or the extraction is done at high frequencies at which the measurement accuracy is limited.

The construction method of a measurement-based model is straightforward. Essentially, the model consists of data tables, in which the output quantity is given for all wanted combinations of the input quantities and/or external conditions. Circuit simulations with data tables are fast and an advantage to manufacturers is that they need not disclose any physical information about the device as it is “hidden” inside the model. However, the measurement effort needed for a well-descriptive model might be excessive, making the size of the data table impractically large. An additional challenge at millimeter wavelengths is the measurement of harmonic frequencies produced in a nonlinear device. For example, building a reliable model of a mixer with a

measurement-based Schottky diode model would require accurate determination of several harmonics. For a millimeter wave mixer this would be extremely difficult and in many cases impossible.

In this thesis, the characterization of Schottky diodes in [V] and [VI] is carried out in an on-wafer environment, and the model for the device includes a measurement-based linear part for the transmission lines as well as a physical model for the nonlinear Schottky junction.

2.4 Simulation Tools

Electromagnetic and circuit simulation tools are necessary for accurate and efficient design of millimeter wave devices. In electromagnetic simulation, the interaction between the electromagnetic field and a physical object and environment is determined by solving Maxwell's equations under specified boundary conditions. Circuit simulation uses mathematical models for passive and active parts of the circuit and calculates the output for a given input stimulus. For the design work done in this thesis, one electromagnetic and one circuit simulator are used extensively, namely, ANSYS HFSS™ [8] and Agilent Advanced Design System (ADS) [9].

HFSS™ is a 3D full-wave electromagnetic simulator software package that uses the finite-element method (FEM) for finding the solution for a given problem. Once the geometry and material parameters are specified, HFSS™ generates a mesh of elements across the structure and solves Maxwell's equations at the mesh nodes. ADS is an electronic design software package offering various features. In this thesis, ADS is used for frequency domain and harmonic balance (HB) circuit simulations of linear and nonlinear circuit elements.

In addition to these electromagnetic and circuit simulators, the MATLAB computing language [10] is used for numerical calculations and parameter extraction as well as in the post processing and presentation of the results.

3 Impedance Tuners

An impedance tuner is a device that changes or "tunes" the impedance seen by a device connected to it. This definition is rather loose, since even a person touching an FM radio antenna for better reception could be considered an impedance tuner. Here, the term is reserved for those devices that are specifically designed for impedance tuning in a controllable manner. Common figures of merit for impedance tuners are the maximum attainable reflection coefficient ρ and the corresponding voltage standing wave ratio *VSWR*. If the voltage standing wave ratio is known, the voltage reflection coefficient can be calculated as follows:

$$|\rho| = \frac{VSWR - 1}{VSWR + 1} \quad . \tag{3.1}$$

Reflection coefficient is often expressed in decibel units. The reflection coefficient in decibels (the absolute value of which is also known as return loss) can be calculated from the voltage reflection coefficient using

$$\rho_{dB} = 20 \log|\rho| \, . \tag{3.2}$$

Other important characteristics of an impedance tuner include smooth phase response, repeatability and resistive loss, which should be as low as possible.

Impedance tuners are used in a variety of applications, including but not limited to device evaluation [11], mixers and multipliers [VIII], [12], [13], waveguide-to-microstrip line transitions [14], noise parameter measurements [15], [16], load-pull measurements [17], [18], and in optimization of high power waveguide systems [19]. In the future, MEMS-based impedance tuners [20]-[22] might find widespread applications, as they can be conveniently fabricated on the same chip with other passive and active circuit elements.

In this chapter, three impedance tuning devices are presented, namely, a multiwaveguide-band backshort and two stub-based waveguide impedance tuners: an *EH*-tuner and a double-stub *E*-plane tuner.

3.1 Waveguide Backshorts

A waveguide backshort (also known as moving short, movable backshort, variable short circuit, waveguide short circuit, or sliding short) is a waveguide circuit element, which provides an adjustable reactive load for the waveguide. Thus the magnitude of the reflection coefficient is ideally one, and the phase is adjusted by moving the position of the backshort. Waveguide backshorts can be roughly divided into contacting and noncontacting backshorts [23].

In contacting backshorts, the metal of the backshort makes a galvanic contact with the metal walls of the waveguide. This can be achieved, for example, by snugly fitting a piece of metal into the waveguide or by using a "springy" metal structure. Metal-to-metal contact causes wear to both the backshort and to the waveguide, making these structures unreliable in repeatable use. The tight machining tolerances for the snug fit cause additional problems at higher millimeter wave frequencies. In [24], a cam-based design is presented, which provides excellent performance at X-band (8-12 GHz) frequencies. The shorting plunger moves in the waveguide without wear and when the contact is made, the cam is forced open, jamming it to the waveguide walls and providing a reliable short circuit. Due to the mechanical tolerances of the moving parts, this design is not scalable to high millimeter wave frequencies.

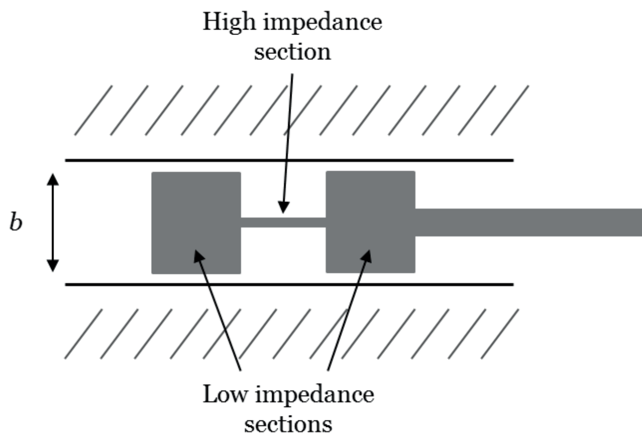

Figure 3. Illustration of the noncontacting backshort concept. The backshort consists of high and low impedance sections. Waveguide height is b.

The problems associated with contacting backshorts at millimeter wavelengths have led to the development of noncontacting backshort designs. The idea is simple: a filter structure inserted into a waveguide reflects the incident signal. Practically all noncontacting backshorts employ a low-pass filter consisting of low impedance/high impedance sections, as illustrated in Figure 3. The sections can be rectangular [25]-[28] or dumbbell-style [29]-[31] plungers, or they can be cut into a metal bar to increase the rigidity of the backshort [32]-[34]. In such structures, “noncontacting” means that there is no galvanic contact between the metal walls of the waveguide and the conducting backshort structure. However, there can be (and usually is) an insulator material between the backshort and waveguide walls. The insulator can be, for example, a thin mylar tape or evaporated silicon dioxide (SiO_2) film.

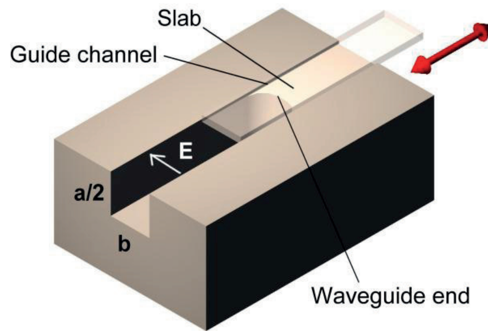

Figure 4. Operating principle of the dielectric-based backshort [39].

A fair comparison of the designs presented above is difficult, as most measurements are performed using scale models, or the performance of the backshort is demonstrated by using it in a working device, such as a mixer. However, in [27], a design covering the W-band (75-110 GHz) with less than 0.3 dB of return loss was reported, and approximately the same performance was achieved in [33] across the 76-90 GHz band. In [28], noncontacting backshorts are fabricated using a new approach, in which a micromachined periodic plunger was found at 220-325 GHz to have a return loss of less than 1.0 dB across the band, with the exception of some point frequencies at which a resonance occurred.

It is also possible to fabricate the filter into a planar metal plate [35] or on a dielectric substrate [36] using photolithographic processes. In [36], a return loss of less than 0.2 dB was measured between 50-63 GHz. Common challenges for the filter-based backshorts include the suppression of resonances inside the operation band, stringent machining tolerances of the waveguide and the filter structure, fragility of the high impedance section and the positioning (distance from waveguide walls and tilt) of the backshort.

A novel dielectric-based backshort for the W-band is presented in [37]-[39]. The backshort is based on a fixed metal short circuit and in a dielectric slab. The dielectric slab is inserted into the waveguide through a rectangular hole in the *E*-plane direction in a fixed metal backshort of the waveguide. The rectangular hole is dimensioned to have its cut-off frequency above the operation frequency of the waveguide TE_{10} mode. The operating principle is illustrated in Figure 4. Return loss of less than 0.21 dB was achieved over the entire W-band [38].

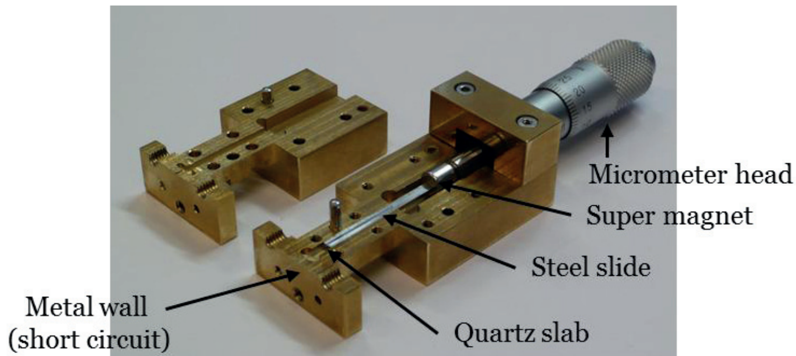

Figure 5. Photograph of the multiwaveguide-band backshort. The upper split-waveguide block is shown on the left hand side.

3.1.1 Multiwaveguide-Band Backshort

Paper [II] presents a waveguide backshort that is compatible with several different-sized waveguides with the same standard flange interface. The operation principle of the backshort is the same as presented in [38] and [39]: the moving dielectric slab

changes the propagation constant and thus the reflection phase of the waveguide it is attached to.

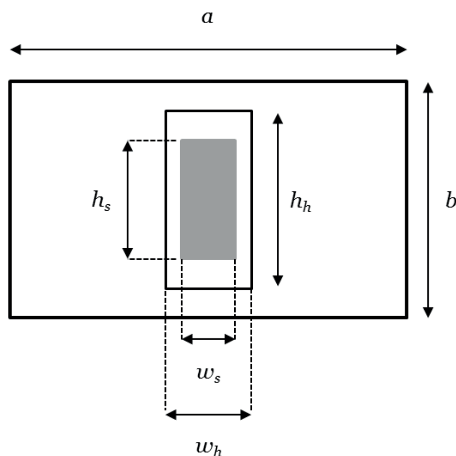

Figure 6. Positioning of the rectangular hole and the dielectric slab with respect to the waveguide.

A photograph of the multiwaveguide-band backshort structure is shown in Figure 5. It consists of upper and lower split-waveguide blocks. A micrometer head is attached to the lower block, and a super magnet is in turn attached to the spindle of the micrometer. The super magnet makes a strong contact with a steel slide, on which a thin dielectric slab is attached with wax. When the micrometer is adjusted, the slab moves in and out of the rectangular hole in the metal wall, which is the fixed short circuit of the waveguide that the backshort is attached to. A cross-sectional view of the rectangular hole and the dielectric slab in the waveguide is shown in Figure 6. The waveguide width is a and height b, rectangular hole height is h_h and width w_h, and the height of the dielectric slab is h_s and width w_s.

The multiwaveguide-band backshort differs in two respects from the design in [38]. First, the waveguide part of the backshort is removed leaving only a smooth metal surface with a rectangular hole and standard flange interface. This enables the backshort to be utilized with all waveguide sizes having the same flange interface and a height larger than that of the dielectric slab. Second, the dielectric slab height in the multiwaveguide-band backshort is less than that of the waveguide. This makes it

possible to dimension the rectangular hole and the dielectric slab in a way that also the waveguide TE_{01} mode is in the cut-off within the rectangular hole. This feature becomes more important when the backshort is scaled to ever higher frequencies, and a possible misalignment of the backshort unit or the dielectric slab would enable the coupling of power from the TE_{10} mode to the TE_{01} mode which could then propagate in the dielectric-filled rectangular hole.

An approximation for the reflection coefficient phase as a function of the dielectric slab length in the waveguide can be calculated using

$$\varphi = \pi - 4\pi \left[\frac{1}{\lambda_{g,diel}} - \frac{1}{\lambda_g} \right] \cdot l \,, \tag{3.3}$$

where λ_g is the wavelength in the empty waveguide, $\lambda_{g,\ diel}$ is the wavelength in the waveguide with dielectric, and l is the length of the dielectric slab inserted into the waveguide. Equation (3.3) indicates linear phase change as a function of the slab length. However, this is not strictly the case, as some interference is caused by two reflected waves, one from the fixed metal backshort and the other from the discontinuity at the interface between the empty waveguide and the waveguide with the dielectric. The result of the interference is a smooth ripple in the reflection phase.

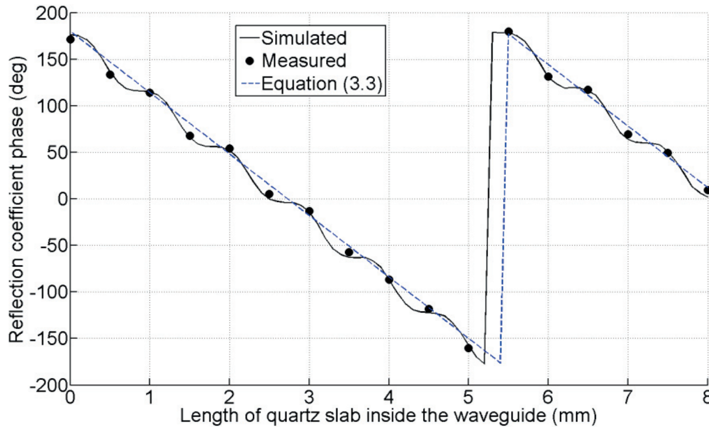

Figure 7. Reflection coefficient phase at 180 GHz as a function of the quartz slab length inserted into the WR-5 waveguide.

The reflection phase changes smoothly, but not linearly as a function of the quartz slab length in the waveguide. For example, the phase change at 180 GHz is shown in Figure 7. The measured phase change for dielectric slab length of 5.0 mm is 332°. In comparison, using (3.3) with a simulated wavelength in the waveguide, $\lambda_{g,\ diel}$ = 1.81 mm, the calculated phase change is 330°. [1]Concerning the sensitivity of the multiwaveguide-band backshort to the dimensions or positioning of the dielectric slab: full-wave simulations show that at the center frequency of the W-band, 92.5 GHz, and with the maximum 8 mm insertion of the slab into the waveguide, a 2 % fabrication error in the thickness or in the width of the quartz slab or the placing of the slab anywhere in the guide channel (rectangular hole in Figure 6) changes the absolute phase less than 2 degrees.

The losses of the multiwaveguide-band backshort are caused by the metal wall (brass) and the dielectric slab (quartz). As the reflection from the metal wall is very low loss and the loss tangent of quartz is around tan θ = 0.0001-0.0004, the overall losses from the structure are small, estimated to be less than 0.05 dB at the W-band and less than 0.25 dB at the D- and G-bands. A maximum reflection coefficient larger than 0.972 ($VSWR$ > 70) is measured at the center frequencies of the D- and G-band (140 GHz and 180 GHz), and larger than 0.988 ($VSWR$ > 165) at the center frequency of the W-band (92 GHz) for any length of the quartz slab between 0 - 8 mm. The main contributor to the overall loss comes from the waveguide section which is used with the backshort and hence depends on the waveguide size and quality used.

In addition to the low losses and the compatibility with several waveguide sizes, the backshort unit provides resonance-free operation and high-resolution tuning. As an example of the latter, the backshort phase response at the W-band is examined more closely. The total phase change for the insertion of quartz from zero to 8 mm is 66° at 92 GHz, corresponding to an average phase change of 0.0825°/10 µm. Compared with a traditional backshort, this phase change would be 0.847°/10 µm. However, one drawback in the dielectric-based backshort concept is the phase response, which is slightly nonlinear and experiences rapid change as a function of frequency. Due to this rapid phase change, the backshort is best suited for narrow-band applications.

---

[1] A more in-depth sensitivity analysis for the glass-like material in Paper [IV] was presented in GSMM2010 but not published.

An important feature of the multiwaveguide-band backshort is its straightforward scalability to higher frequencies. Basically, the backshort works as long as the cut-off frequency of the rectangular hole with the dielectric material is above the operating frequency of the waveguide that it is attached to. As an example, a square shaped quartz slab with a side length of 50 μm and a square hole with a side length of 80 μm is within the capabilities of current milling and laser cutting equipment. This structure has a cut-off frequency of ~1.34 THz and could therefore be used with a WR-1 waveguide (a = 254 μm, b = 127 μm) in the frequency band of 750-1100 GHz.

3.2 Sliding Screw- and Stub-Based Waveguide Impedance Tuners

Millimeter wave waveguide impedance tuners are based on the "sliding-screw" or stub approaches [11]-[16], [23], [40]-[42], although a more descriptive alternative name for the "sliding-screw" would be a "sliding-probe" approach at millimeter wavelengths. Sliding-screw tuners are commercially available at least to 110 GHz [43], and stub-based waveguide tuners cover the entire millimeter wave range [44]. In [40] a return loss of 0.3 dB was measured at 60 GHz using an automated *EH*-tuner, while [42] was able to measure a voltage reflection coefficient greater than 0.9 ($VSWR$ > 19) at 75-100 GHz with a sliding-screw tuner. A commercial automated tuner from Maury Microwave Corporation [43] provides insertion loss less than 0.65 dB across the W-band with the tuning probes fully retracted from the waveguide.

Sliding-screw tuners are often bulky, electrically large, and are difficult to scale to higher frequencies as the dimensions of the probe and the opening in the middle of the broad wall of the waveguide should be only a small fraction of the waveguide dimensions. The stub-based tuners, on the other hand suffer from the drawbacks of the waveguide backshorts discussed in Section 3.1. In addition, neither design is readily compatible for integrating components, such as waveguide-to-microstrip line transitions, close to the tuner structure for decreased losses.

In this section, two waveguide impedance tuners are presented, that are designed to address these disadvantages. Both impedance tuners are fabricated using the split-

waveguide block technique, which enables the integration of other millimeter wave components in close proximity of the tuner thus decreasing the resistive losses caused by the extra waveguide sections. Furthermore, both tuners utilize the concept of the dielectric-based backshort presented in [II] and in [37]-[39], which provides a resonance-free, high-resolution and low-loss tuning mechanism.

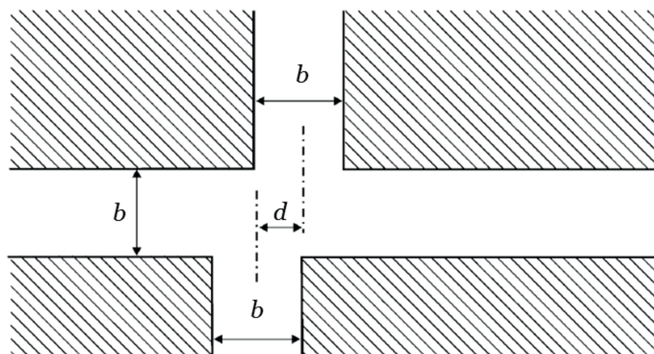

Figure 8. Schematic of the double *E*-plane junction. Tuner arm separation is *d* and waveguide height is *b*.

3.2.1 *E*-plane Double-Stub Tuner for the W-Band

A novel waveguide stub-tuner using two closely-spaced *E*-plane tuning arms for impedance control is presented in [I]. The tuner is optimized to cover the entire W-band with low losses and wide impedance coverage. An illustration of the double *E*-plane junction is shown in Figure 8. *E*-plane junctions have equivalent circuits [45], which could be used with a circuit simulator for design of the tuner. However, as the optimum separation of the tuning arms, d = 0.5 mm ($\lambda_g/13$- $2\lambda_g/13$, 75-110 GHz), is less than the height of the W-band waveguide, b = 1.27 mm, the behavior of the double junction differs somewhat from the behavior of the two well-separated junctions. To obtain the best possible accuracy, the double junction is simulated with a full-wave electromagnetic simulator, ANSYS HFSS™, and the resulting S-parameter file is then embedded into the ADS circuit simulator. The simulations use variable length transmission lines as tunable backshorts.

Because double-stub tuners cannot completely cover the Smith diagram, but always leave an unmatched area [5], the lengths of the main waveguide sections on both sides of the tuner are designed to be different, in order to shift the unmatched area when the tuner is turned around and to achieve maximum combined coverage. The perimeter of the Smith diagram (the resistive part of the load impedance equals zero) can never be covered with any tuner, as some losses are always present.

The performance of the impedance tuner is state-of-the-art in the W-band. For example, the maximum attainable reflection coefficient at the center frequency of the band, 92.5 GHz, is 0.96 (*VSWR* = 49) and the maximum coverage on the Smith diagram (turning around the tuner is needed for full coverage) is 94 %. The simulated and measured coverage without turning the tuner around are shown in Figure 9. The measured coverage is 76 %. As the impedance tuner is fabricated using a traditional machining method, other waveguide components can easily be integrated in close proximity of the tuner for optimal performance and reduced losses.

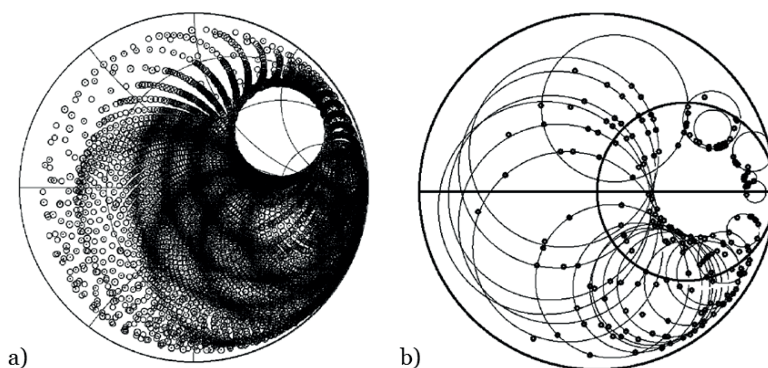

Figure 9. Input impedances of the waveguide impedance tuner at 92.5 GHz for different positions of the dielectric-based backshorts. In a) simulated and in b) measured results are shown. In b) circles show the obtainable impedances.

One drawback of the tuner is the fast, nonlinear phase response as a function of the frequency. In addition, the double *E*-plane approach (stubs are in series) always results in an unmatched area on the Smith diagram. This latter drawback is addressed in the next section, which presents the dielectric backshort-based *EH*-tuner.

In order to demonstrate the low losses of the tuner, the resistive loss is calculated using

$$L_{res} = -10\log\left(|S_{11}|^2 + |S_{21}|^2\right), \tag{3.4}$$

where S_{11} is the reflection coefficient and S_{21} the transmission coefficient. With an ideal lossless tuner, the L_{res} = 0 dB. The resistive loss of the tuner with three different tuner settings is shown in Figure 10. The resistive loss caused by the tuner structure is small, with the median value for the loss for any of the three combinations being between 0.24 – 0.28 dB.

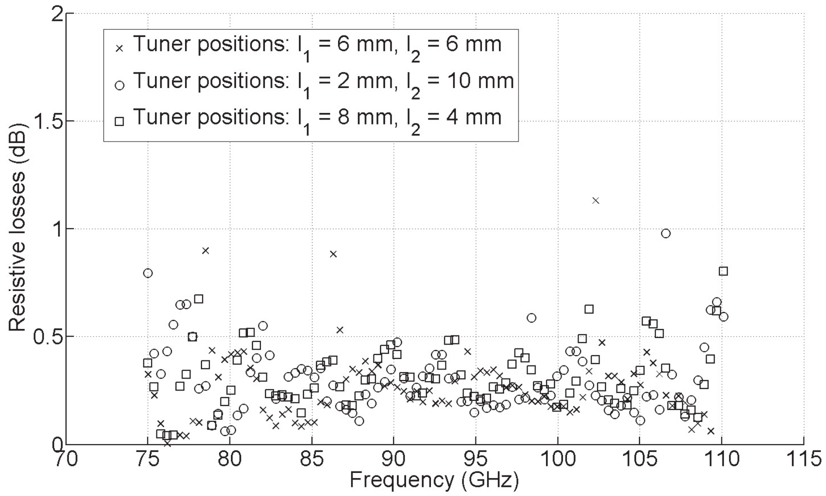

Figure 10. Resistive losses of the *E*-plane tuner with three different positions of the dielectric backshort. Resistive losses are calculated from the measured data using (3.4).

3.2.2 *EH*-Tuner for the G-band

The *EH*-tuner is a classic stub-based waveguide impedance tuner based on the magic-T four-port junction, in which one tuner arm is in series (*E*-plane) and the other lies parallel (*H*-plane) to the main waveguide [5], [46]. A major advantage of the *EH*-tuner is its ability to cover the entire Smith diagram (again, except purely reactive impedances) with just two matching elements. A double-stub tuner, where the tuning elements are both in series or in parallel cannot achieve this. A drawback of the *EH*-tuner is that it has a more complex structure than that of either the *E*- or *H*-plane

double-stub tuner, since a directly machined *EH*-tuner must be fabricated in three parts.

Paper [III] presents an *EH*-tuner using dielectric-based backshorts [II], [37]-[39]. Mechanically, the tuner consists of three blocks, which are separately fabricated and then assembled. As an example, a 3D illustration of one of the blocks is shown in Figure 11. The *E*-plane backshort is machined in the same block with the magic-T junction, and the *H*-plane backshort [II] is connected to the *H*-plane arm using a standard flange interface. The tuner is designed to form part of a waveguide mixer test jig which can test Schottky diodes in their usual operating environment [VIII]. A directly machined *EH*-tuner with dielectric-based backshorts is selected to enable high-resolution tuning, low losses, a maximum range of input impedances, and the possibility to integrate the quartz chip with the diode as close to the tuner as possible. In order to test the performance of this tuner, a stand-alone version presented in [III] is fabricated.

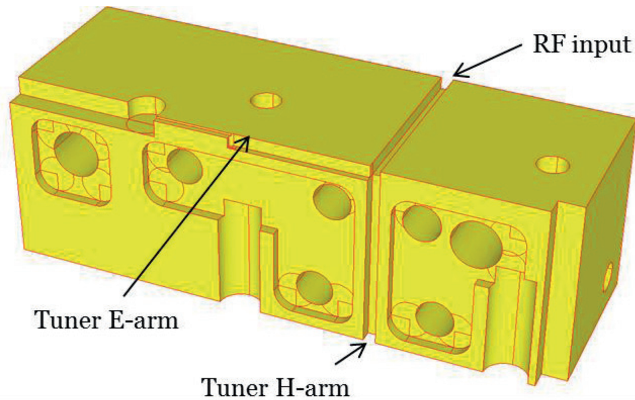

Figure 11. 3D illustration of one of the three parts of the *EH*-tuner. Hollows are machined to ensure high-quality contact at the waveguide intersections.

An estimate for the resistive loss is calculated using (3.4) for three combinations of the dielectric backshort position. The results are shown in Figure 13. The median loss for any of the three combinations is between 0.84 – 0.92 dB. It should be noted here that this loss includes the losses of the input (8 mm) and output (18 mm) waveguides. The length difference is not as necessary in the *EH*-tuner as it is in the double-stub *E*-plane tuner because there is no unmatched area (except for the small resistive parts) on the

Smith diagram. Nevertheless, the length difference is useful for research purposes as it enables the evaluation of the waveguide propagation constant and loss factor.

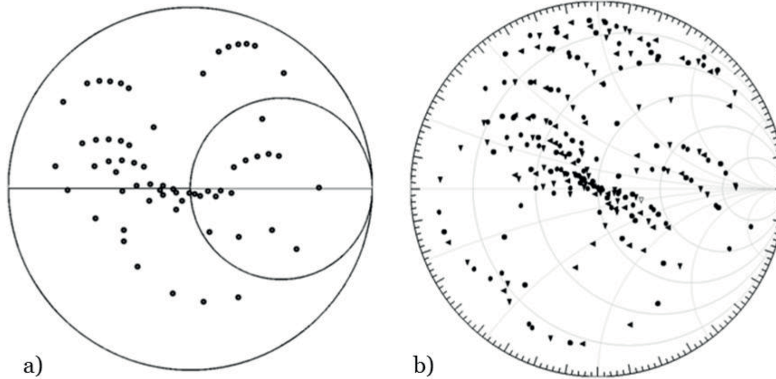

Figure 12. Input impedances of the *EH*-tuner at 183 GHz for different positions of the dielectric-based backshorts. In a) 64 measured and in b) 225 simulated input impedances are shown.

One limitation of this design is its structure, which has a waveguide interface in the middle of one of the narrow walls of the *E*-plane arm. Splitting a waveguide in this plane as opposed to the usual cut in the middle of the broad wall, results in a larger loss. ANSYS HFSS™ simulations and studies in [47] demonstrate that the reflection from the tuning arms and the direct coupling between the input and output port increases with increasing frequency. Thus, in order to match impedances at the higher frequency of the operation band, stronger resonances (larger *VSWR*) are needed from the tuning arms. Larger resonances increase the current flow and thus increase the resistive loss of the structure. Future *EH*-tuner designs should therefore aim to improve the operation of the magic-T junction, e.g., by matching the junction as in [47] or by decreasing the size of the waveguides from the standard size (the cut-off frequency must obviously be below the lowest operating frequency of the band).

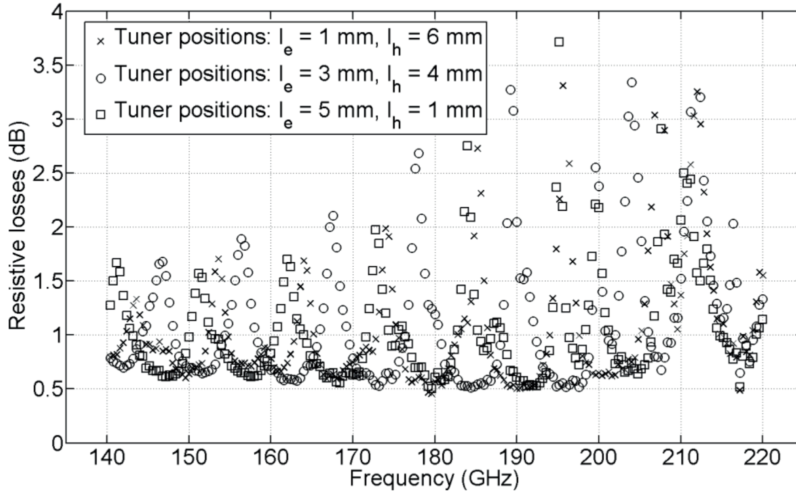

Figure 13. Resistive losses of the *EH*-tuner with three different positions of the dielectric backshorts. Resistive losses are calculated from the measured data using (3.4).

3.3 Short Summary and Discussion on Waveguide Impedance Tuners

This chapter examines the literature on waveguide backshorts and waveguide impedance tuners. In addition, three impedance transforming devices developed in the work are presented, namely, a backshort unit, compatible with several different waveguide sizes [II] and two stub-impedance tuners for the waveguide environment: an *E*-plane double-stub tuner for the W-band [I] and, an *EH*-tuner for the G-band [III]. Both impedance tuners utilize the same dielectric backshort concept that forms the base for the operation of the multiwaveguide-band backshort.

All three devices are fabricated using the split-waveguide block technique and provide several advantages over current state-of-the-art waveguide tuners, including low losses, no resonance behavior from the backshort unit, high-resolution tuning, and the ability to integrate other waveguide components, such as microstrip line transitions, in close proximity to the tuner. In addition, the operation of the dielectric-based backshort is not compromised by an error in the positioning of the dielectric slab nor by the

fabrication tolerances in the dimensions of the slab or the waveguide with which it is used. This means that the absolute phase response will obviously be different with a different sized dielectric slab or waveguide, but the operation of the backshort unit as a high-reflection load is not compromised as is the case for traditional noncontacting backshorts, where small manufacturing errors might cause significant resonances at the operation band.

Scaling of the multiwaveguide-band backshort and the impedance tuners is much easier than that of the traditional backshorts, as snug fit or micrometer precision in the dimensions of the backshort parts is not necessary for the correct operation of the dielectric-based backshort.

For the multiwaveguide-band backshort, the measured maximum reflection coefficient is larger than 0.972 (*VSWR* > 70) at the center frequencies of D- and G-band (140 GHz and 180 GHz), and larger than 0.988 (*VSWR* > 165) at the center frequency of W-band (92 GHz) for any length of the quartz slab between 0 - 8 mm. For the double-stub *E*-plane tuner, the maximum attainable reflection coefficient at the center frequency of the band, 92.5 GHz, is 0.96 (*VSWR* = 49) and the maximum coverage on the Smith diagram (turning around the tuner is needed for full coverage) is 94 %. The median resistive loss ranges between 0.24-0.28 dB, depending on which of the three measured combination of the backshorts position is used.

The maximum obtained reflection coefficient for the *EH*-tuner is 0.92 (*VSWR* = 24) and 0.875 (*VSWR* = 15) at 148 GHz and at the nominal design frequency of the mixer test jig [VIII], 183 GHz, respectively. The median resistive loss for the *EH*-tuner ranges between 0.84-0.92 dB, depending on which of the three measured combination of the backshorts positions is used.

The drawbacks of these designs are related to the backshort. Since the phase change as a function of the dielectric slab length in the waveguide is slower than that of the movement of traditional backshort, the waveguide length needed is larger. For the same reason, the phase response of the dielectric-based backshort is fast and not linear. As a result, the multiwaveguide-band backshort and the impedance tuners are best suited for narrow-band applications.

4 Schottky Diode

The rectifying phenomenon of a metal-semiconductor junction was discovered already in 1874 by F. Braun [48]. This was almost 60 years before the transport theory of semiconductors was created by A. H. Wilson [49]. Today, the component based on the metal-semiconductor junction is called a Schottky diode after W. Schottky, an early developer of the physical model for the device [50]. Other early developers include N. F. Mott [51] and H. F. Bethe. Following this pioneering work, the theory has been enhanced and expanded by various scientists. Notable names include A. M. Cowley, S. M. Sze, A. Padovani, R. Stratton, C. R. Crowell, and V. L. Rideout, [52]-[55].

This chapter briefly describes the basic operating principles of the Schottky diode and explains the modeling and characterization methods relevant to this work. This work focuses on RF applications. The pertinent semiconductor physics and theory are briefly discussed and references are given for a comprehensive overview.

4.1 Fundamentals of the Schottky Diode

Schottky diodes can be divided into resistive (varistor) and varactor diodes. In a resistive device, the frequency conversion is based on resistance modulation. A varactor is a variable capacitance device in which the frequency conversion is based on capacitance modulation. Resistive diodes are used as mixers, detectors and frequency multipliers, and varactor diodes as frequency multipliers. A frequency multiplier based on a resistive Schottky diode has a lower maximum efficiency than its varactor counterpart, but can cover a wider range of frequencies. On the other hand, varactor multipliers can produce high efficiencies and output powers, and have higher breakdown voltages than resistive multipliers, indicating that they can be driven with larger input power levels. Although the work presented in this thesis and the appended papers [V]-[VIII] focuses only on resistive diodes, most of the discussion in this chapter related to physics, modeling and the characterization of Schottky diodes is applicable to both resistive and varactor diodes.

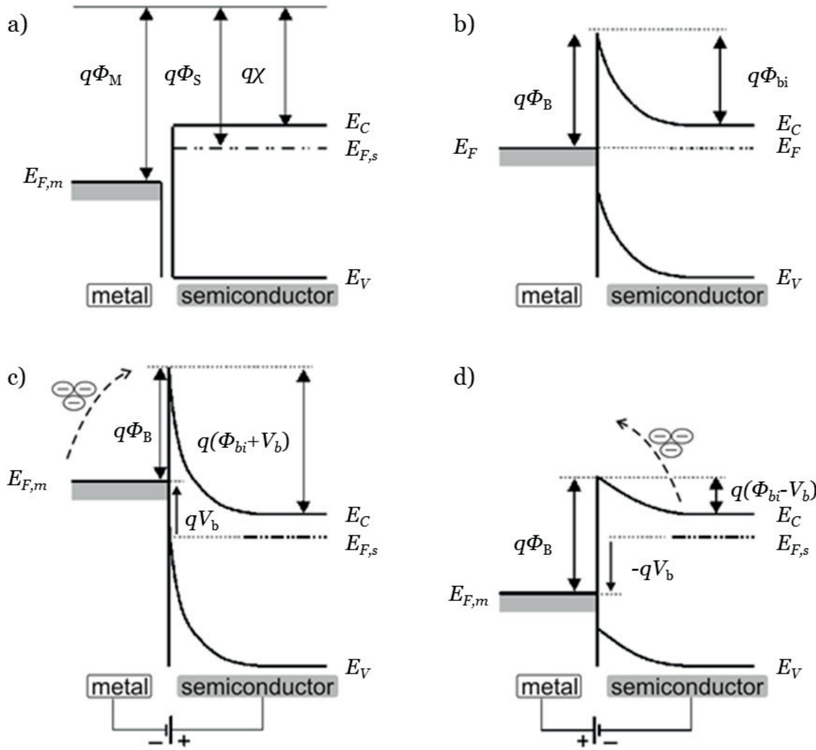

Figure 14. Energy band diagram of metal-semiconductor (n-type) contact. In a) metal and semiconductor are not in contact, in b) metal and semiconductor are connected and form a single system, in c) metal-semiconductor junction is reverse biased, and in d) metal-semiconductor junction is forward biased. According to [60].

4.1.1 Barrier Formation

The potential barrier that is formed between a metal and semiconductor once they are in contact is responsible for the Schottky diode current-voltage (I-V) and capacitance-voltage (C-V) characteristics. This section briefly discusses the physics behind the barrier formation and operation under bias voltage. Only the case of an ideal junction is considered, and several effects are ignored, such as those caused by the interfacial layer and image-force lowering. An in-depth discussion on the physics and operation of the Schottky diode is given, e.g., in [56]-[59].

The energy band diagram for a metal-semiconductor (n-type) interface according to [60] is shown in Figure 14. Four different cases are shown, illustrating the situations where the materials are separated, in contact, in contact with reverse bias, and in contact with forward bias.

In the case where the metal and n-type semiconductor are not in contact, the Fermi level in the semiconductor, $E_{F,s}$, is higher than that of the metal, $E_{F,m}$. The work function is the energy difference between the Fermi level and the vacuum energy. This is denoted as $q\Phi_M$ for the metal and $q\Phi_S$ for the semiconductor. The energy level between the conduction band of the semiconductor and the vacuum energy is $q\chi$, where χ is the electron affinity.

Once the contact is made, electrons flow from the semiconductor to the metal until the created electrostatic potential compensates for the difference in the original Fermi energies. As a result, the Fermi level in the semiconductor is lowered to the same level as the Fermi level in the metal, E_F, and the flow of electrons stops. The accumulated electrons on the metal surface of the interface have created (or built) a potential barrier for the electrons in the semiconductor. This barrier is called the built-in voltage (also called the diffusion voltage) and can be calculated simply with

$$q\Phi_{bi} = q(\Phi_M - \Phi_S)\,. \qquad (4.1)$$

Similarly, the electrons in the metal also experience a potential barrier with the height of

$$q\Phi_B = q(\Phi_M - \chi)\,, \qquad (4.2)$$

which is known as the Schottky barrier. The flow of electrons from the semiconductor to the metal causes part of the semiconductor to gain a positive net charge. This positively charged area is called the depletion region. The width of the region, the depletion width w_d, is an important parameter for the operation of the junction.

The Schottky junction can be biased in two ways. In reverse biasing (Figure 14 c), the semiconductor side of the junction is connected to a positive voltage and the side of the metal to a negative voltage. For forward biasing, the polarity of the voltage is changed

(Figure 14 d). In the former case, the energy of the electrons in the semiconductor is decreased by $q|V_b|$, where V_b is the applied voltage or the bias voltage. In forward biasing, the energy is increased by the same quantity. Electrons with less energy are less likely to move across the potential barrier than are the electrons with more energy. Consequently, the current through the junction increases with an increasing bias voltage. The width of the depletion region under different bias voltages can be calculated with

$$w_d = \sqrt{\frac{2\varepsilon_s(\Phi_{bi} - V_b - kT_J/q)}{qN_D}}, \tag{4.3}$$

where k is the Boltzmann's constant, T_J is the temperature of the junction, N_D is the donor doping density, and ε_s is the permittivity of the semiconductor material that can be expressed as $\varepsilon_o\varepsilon_r$, where ε_o is the permittivity of vacuum and ε_r is the dielectric constant of the semiconductor.

4.1.2 Current-Voltage Characteristics

The dominant current transport mechanisms in state-of-the-art GaAs Schottky mixer diodes are the emission of electrons over the barrier and the quantum mechanical tunneling of electrons through the barrier. A widely recognized model which takes into account both of these effects is the thermionic-field emission model [53], [56]-[59]. Generalized I-V characteristics can be written in the form

$$I = I_S\left[\exp\left[\frac{q(V_b - IR_S)}{\eta kT_J}\right] - 1\right] \approx I_S \exp\left[\frac{q(V_b - IR_S)}{\eta kT_J}\right]. \tag{4.4}$$

Here I_S is the saturation current, η is the ideality factor, and R_S is the series resistance of the diode. Temperature dependence of the saturation current and ideality factor can be expressed as

$$I_S = SA^{**}T_J^2 \exp\left[\frac{-q\Phi_B}{\eta kT_J}\right] \tag{4.5}$$

$$\eta = \frac{q}{kT_J} E_{00} \coth\left[\frac{qE_{00}}{kT_J}\right], \tag{4.6}$$

where S is the junction area, A^{**} is the modified Richardson constant (8.2 $Acm^{-2}K^{-2}$ for GaAs), and E_{oo} is a constant with a constant doping density. For now, the series resistance is assumed to have a constant value.

The thermal dependence of the saturation current and ideality factor is important, as all Schottky diodes experience self-heating effect caused by the bias current. According to [58], [59] and [61], the temperature of the junction can be estimated using

$$T_J = T_0 + P_T R_\theta , \tag{4.7}$$

where T_o is the ambient temperature, P_T is the power dissipated in the junction, and R_θ is the thermal (spreading) resistance of the diode. Assuming that most of the power is dissipated in the junction, P_T can be evaluated with

$$P_T = V_b I . \tag{4.8}$$

For round anodes, an estimate for the thermal resistance can be calculated with

$$R_\theta = \frac{\rho_\theta}{4r_a}, \tag{4.9}$$

where ρ_θ is the thermal resistivity and r_a is the anode radius. At 300 K, the thermal resistivity for GaAs is $\sim 22 \cdot 10^{-3}$ Km/W [62]. It should be noted that (4.9) is an approximation for the situation in which the semiconductor continues indefinitely far from the junction. For a Schottky diode, the thermal resistance is also determined by other materials close to the junction and the geometrical structure of the diode. Consequently, the thermal resistance is heavily affected, for example, by the removal of the semiconductor material around the anode or the metallization of the anode finger. Removing material around the anode increases the thermal resistance, while depositing metal on the anode decreases it as metal is a good thermal conductor.

4.1.3 Capacitance-Voltage Characteristics

In addition to its current-voltage characteristics, the Schottky junction also exhibits a voltage dependent capacitance behavior. The capacitance is caused by the accumulated charge on both sides of the depletion region. The size of the capacitor depends on the junction size, doping density, and applied voltage and can be calculated with

$$C_j = S\left[\frac{q\varepsilon_s N_D}{2(\Phi_{bi} - V_b - kT_J / q)}\right]^{\frac{1}{2}}. \tag{4.10}$$

After some algebraic manipulation and neglecting the term kT_J/q, this can be expressed as the well-known Schottky diode C-V equation

$$C_j = \frac{C_{j0}}{[1 - V_b / \Phi_{bi}]^{\frac{1}{2}}}, \tag{4.11}$$

where C_{jo} is the zero-bias junction capacitance. The exponent 0.5 is only valid for uniform doping of the junction. This is a reasonable assumption for GaAs Schottky mixer diodes, such as those used in this work. Although not strictly valid, (4.11) is a good approximation for the C-V behavior of the junction and is widely used in the parameter extraction and in the circuit analysis of Schottky devices [63], [64].

4.1.4 Frequency Conversion

Essentially all millimeter wave applications of Schottky diodes are based on its nonlinear I-V characteristics (or C-V characteristics in the case of varactor diodes) and the consequent ability to perform frequency conversion of signals. To illustrate this, a simplified version of (4.4) is used to calculate the time-dependent junction conductance waveform under the sinusoidal signal $V = V_o \cos(\omega t)$.

$$I = I_S \exp\left[\frac{q(V_b - IR_S)}{\eta k T_J}\right] \approx I_S \exp(\alpha V). \tag{4.12}$$

Here R_S is assumed to be zero and $\alpha = q/(\eta kT_J)$. With this notation the time dependent (small signal) junction conductance is

$$g_j = \frac{1}{r_j} = \frac{dI}{dV} = \alpha I_S \exp\left[\alpha V_0 \cos(\omega t)\right] = \alpha I \ , \tag{4.13}$$

where r_j is the (small signal) junction resistance. Using the series expansion, this can be expressed as

$$g_j \approx \alpha I_S \left[1 + \alpha V_0 \cos(\omega t) + \frac{(\alpha V_0)^2 \cos^2(\omega t)}{2!} + \ldots\right]. \tag{4.14}$$

The first term inside the parenthesis is the direct current (DC) term, which forms the basis for using the Schottky diode as a direct detector. The second and subsequent terms relate to the harmonics of the fundamental signal which enable frequency multiplier applications. Similarly, if two signals with different frequencies are applied, all the sum and difference frequencies are generated ($f_{n,m} = \pm n f_1 \pm m f_2$, n, m = [0, 1, ...]) and the Schottky diode can be used as a down- or up-conversion device, also known as a mixer.

4.2 Schottky Diode Modeling

A fundamental requirement for reliable device design in electrical engineering is having accurate models for both active and passive devices. Generally, a model is a mathematical description of the component which can be attached to other components to create a network of components, i.e., circuits. Models can be roughly divided into linear and nonlinear models, as explained in Section 2.3. Active devices, such as Schottky diodes, consist of both linear and nonlinear parts. In a Schottky diode, the nonlinear part is the metal semiconductor junction, and the linear part contains everything else. This section discusses the modeling approaches commonly used in the design of Schottky diode applications for millimeter wavelengths. These include the physical modeling of the junction, equivalent circuit approach, full-wave modeling and the combination of physical modeling and full-wave modeling.

4.2.1 Physical Modeling of the Schottky Junction

The core of a Schottky diode is the metal-semiconductor junction with its nonlinear I-V and C-V characteristics introduced in Section 4.1. By far the most common way of modeling the junction is a parallel combination of a nonlinear resistor (or conductance) and a nonlinear capacitor. A standard convention is to include a series resistor in this model, even though it is usually considered to be a constant parameter. The reason for this is that a major part of the series resistance is caused by the undepleted epilayer which is part of the junction. A lumped component circuit model for the junction is shown in Figure 15. The I-V and C-V characteristics of the junction models used in the circuit simulators typically follow closely those given by (4.4) and (4.11), although the circuit simulator models may consist of tens of parameters. A myriad of publications have concentrated on theoretical research concerning the Schottky junction, such as [50]-[55] and [65], [66]. Recently, physics-based modeling of the junction, taking into account various physical effects, has produced valuable and experimentally verified results [67], [68].

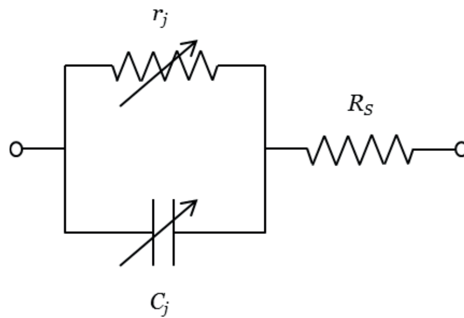

Figure 15. Simple lumped element circuit model for the Schottky junction.

4.2.2 Equivalent Circuit Approach

The junction model alone is not sufficient for designing Schottky-based devices, such as mixers or frequency multipliers, even though the quality of the junction sets the fundamental limits for the performance of such devices. In order to take into account the effect of the linear part of the diode, an equivalent circuit model can be constructed.

The equivalent circuit depends on the type of the diode and on the surrounding circuit. Figure 16 shows an example of an equivalent circuit for a discrete planar Schottky diode mounted on a coplanar waveguide (CPW) environment in the ADS circuit simulator. In addition to the diode junction model (shown as a blue rectangle) the equivalent circuit contains parasitic pad-to-pad capacitance C_p, anode finger inductance L_{ind}, capacitances from the pad edges to ground, C_{g1} and C_{g2}, and small pieces of CPW line to take into account the soldering pads. The equivalent circuit approach is possibly the most common way of designing microwave integrated circuits (MIC) and monolithic microwave integrated circuits (MMIC).

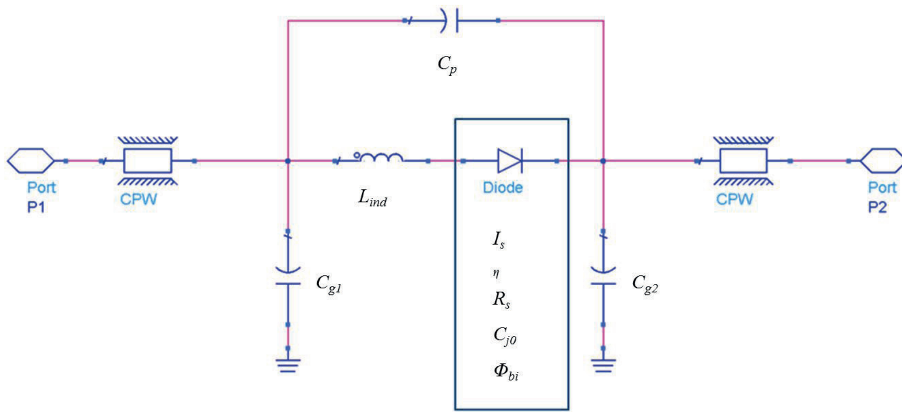

Figure 16. Equivalent circuit for a Schottky diode connected to a coplanar waveguide transmission line.

4.2.3 Full-Wave Modeling

One drawback in the equivalent circuit approach is that it requires the use of circuit elements with well-known mathematical description. If a designer wishes to use custom building blocks to save die area or to improve the performance of a device, it is necessary to create a model for the new block. Furthermore, equivalent circuits rarely take into account the cross-coupling effects between different parts of the circuit, which might be significant, especially in densely packed MMIC applications.

An alternative to the equivalent circuit approach is to use a 3D electromagnetic full-wave simulator, such as ANSYS HFSS™. The circuit or circuit element is built to resemble its real-world counterpart as accurately as possible. After defining the geometry, various material parameters can be associated with the desired parts of the circuit, including dielectric constant, loss tangent, surface impedance, and conductivity. Input and output ports, i.e., the regions where the signal enters and exits of the device, are defined and a steady-state solution is calculated using Maxwell's equations. Full-wave modeling is also an efficient method for investigating the parasitic effects in Schottky devices [69]. However, the full-wave approach can only be used to model linear circuits and not nonlinear physical parts, such as the Schottky junction.

4.2.4 Combined Circuit Simulation and Full-Wave Approach

When building millimeter wave Schottky devices, such as mixers and multipliers, full-wave simulators are frequently used together with circuit simulators in order to achieve the best possible accuracy and first-pass success. This approach has, in many cases, replaced the long-standing trial-and-error and large-scale model experiments [70], [71], making the circuit design cheaper and more efficient.

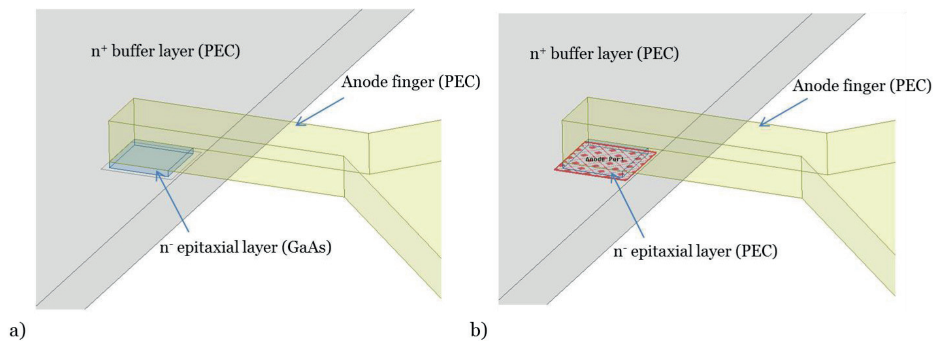

Figure 17. Schottky port definition for connecting the physical junction model correctly. In a) an actual GaAs epilayer and in b) the coaxial port where the junction model will be connected in the circuit simulator.

A nontrivial challenge is to determine a way to couple the full-wave simulator to the circuit simulator. A widely used method in the millimeter- and submillimeter wave Schottky community is described in detail in [72] and used, for example, in [73]-[75]

and in [VII], [VIII]. In short, the linear part of the circuit is simulated in a full-wave simulator, where a small coaxial port is connected in place of the diode junction. The S-parameters calculated from the linear circuit are then exported to the circuit simulator, where the physical model for the junction is connected to the coaxial port. Harmonic balance simulations are then performed to predict the operation of the circuit.

Figure 17 shows an illustration defining the coaxial port. Only a heavily doped buffer layer (n^+), anode finger, and epitaxial layer (n^-) are shown for clarity. A perfect electric conductor (PEC) is used in defining the port to isolate the effect of the port itself and the surrounding circuit. However, in actual device simulations more realistic results are achieved by assigning the materials a loss tangent, surface impedance, or conductivity.

4.3 Schottky Diode Measurements

Several discrete and monolithically integrated Schottky diodes are tested, characterized, and modeled during the research work for this thesis. The main results are discussed in detail in [V]-[VIII].

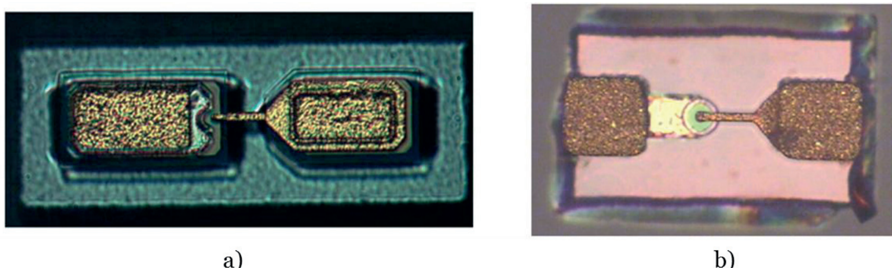

a) b)

Figure 18. Micrographs of the a) VDI-SC2T6 and b) ACST-1MSQ08 single anode Schottky diodes.

Discrete diode types used in this work are a single anode Schottky diode 1MSQ08 from Advanced Compound Semiconductor Technologies (ACST), Darmstadt, Germany [76] and a single anode Schottky diode SC2T6 from Virginia Diodes Inc. (VDI), Virginia, USA [77]. The anode radii are approximately 0.4 µm for the IMSQ08 diode and 0.7 µm for the SC2T6 diode indicating that the diodes are optimized for operation at high

millimeter wave and THz frequencies. Micrographs of the diodes are shown in Figure 18. The monolithic diodes are fabricated using the United Monolithic Semiconductors (UMS) Buried Epitaxial Schottky (BES) process. The monolithic diodes used in the work range in size between 1x3 - 1x20 μm, although different-sized diodes are also tested for comparison purposes.

For the tests, the discrete diodes are soldered on CPW test mounts. In the case of the monolithic diodes, the test mounts are fabricated in the same process with the diodes. An empty discrete diode test mount, a soldered discrete diode, and a monolithically integrated test structure with the diode are shown in Figure 19. The CPW environment is used in the tests, as it enables easy and reliable testing with ground-signal-ground (GSG) on-wafer probes. The test setup for I-V and the S-parameter measurements is shown in Figure 20. In C-V measurements, the contact to the CPW center conductors is done using thin phosphor-bronze whiskers.

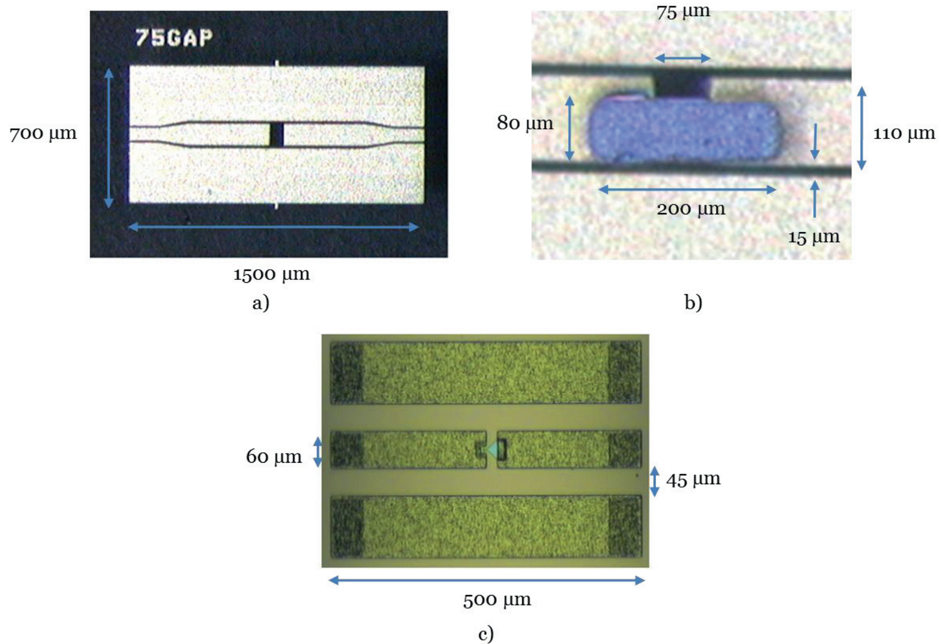

Figure 19. CPW test structures. In a) a test mount for discrete Schottky diodes, in b) a VDI-SC2T6 diode attached to the test mount, and in c) a monolithic UMS Schottky diode with anode width of 5 μm in a CPW test mount.

Most of the measurements are done using the same set of equipment. The S-parameters are measured using an Agilent N5250 PNA between 0.1-110 GHz, I-V parameters and biasing of the diodes for S-parameter measurements are performed with an Agilent 4156C Precision Semiconductor Parameter Analyzer, and C-V measurements using an Agilent 4284A Precision LCR Meter. Temperature controlled I-V and S-parameter measurements are done on a Temptronic Corporation Thermal Platform.

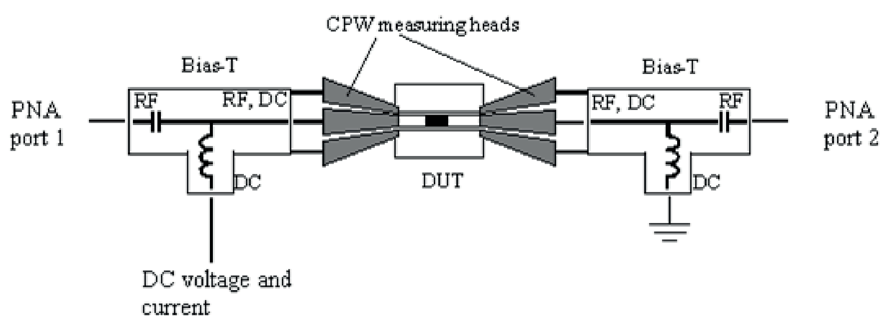

Figure 20. Test setup for I-V and S-parameter measurements.

4.4 Schottky Diode Characterization and Parameter Extraction

This section introduces the conventional I-V, C-V, and S-parameter characterization methods and briefly discusses some general methods for thermal characterization.

4.4.1 I-V Parameter Extraction

The most common characterization and testing method for Schottky diodes is the I-V parameter extraction. This method first performs current-voltage measurements and then extracts the I-V parameters, ideality factor, saturation current, and series resistance, by fitting (4.4) or some auxiliary function derived from (4.4) to the measured results. Occasionally, instead of the saturation current, the Schottky barrier height is extracted by substituting (4.5) to (4.4). However, this requires *a priori*

knowledge of the junction area or the introduction of another unknown parameter, the junction area multiplied by the modified Richardson constant SA^{**}.

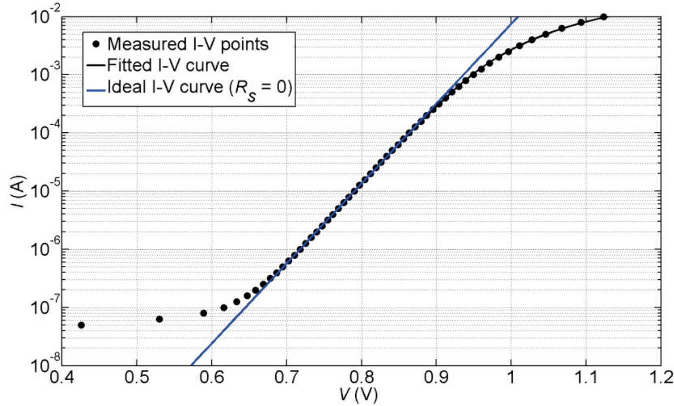

Figure 21. I-V extraction using least-squares fitting algorithm. Measured I-V points and fitted I-V curve with and without the effect of the series resistance. The data is for an SC2T6 diode.

The available literature describing I-V parameter extraction is vast. A widely-used approach is the DC measurement using, for example, a semiconductor (parameter) analyzer or a swept voltage/current source [79]-[89]. As an example, measured I-V characteristics, (least-squares) fitted I-V curve (4.4), and so-called "ideal" I-V curve without the effect of the series resistance are shown in Figure 21.

Although the measured I-V points and the fitted model are visually in excellent agreement, this approach has an inherent limitation that has severe consequences when applied to diodes optimized for high millimeter wave and THz frequencies and have anode diameter less than ~1.0 μm. The limitation is that the algorithm assumes constant temperature during the extraction process and that the ideality factor and saturation current will both have constant values across the used current-voltage range. This, however, is not the case. In fact, the bias current heats up the junction according to (4.7), resulting in different saturation current and ideality factor values at different I-V points according to (4.5) and (4.6).

For small diodes, the heating-effect is substantial, and if it is not taken into account, the extracted value for the series resistance will be too small [61], [63], [90], [91]. This is

illustrated in Figure 22, where ΔV_{error} is the voltage difference of the junction calculated with constant saturation current and ideality factor as well as a temperature dependent saturation current (4.5) and ideality factor (4.6), and $\Delta R_{S,error}$ is the corresponding error in the extracted value for series resistance.

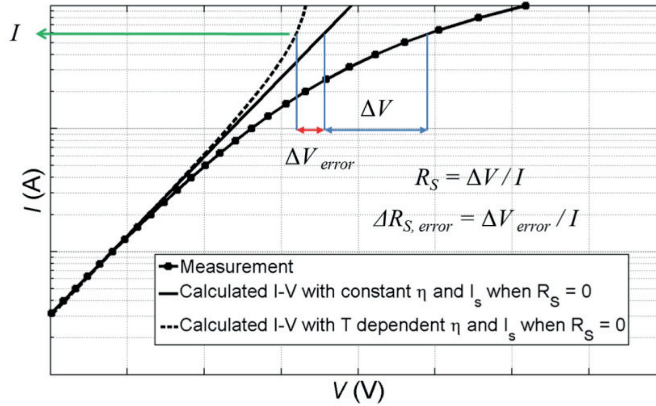

Figure 22. Extraction of the series resistance and the error in the series resistance caused by the temperature dependent saturation current and ideality factor.

The problem described above can be avoided by measuring the I-V characteristics with such a fast signal that the rise time of the signal is less than the thermal time constant of the diode, τ, which can be less than 100 ns for submicron anode Schottky diodes [92]. Such measurements can be conducted, e.g., by using an alternating signal (AC) or pulsed measurements [92]-[96]. The measurement using an AC signal provides a value for the total dynamic resistance of the diode. The junction temperature and value for the ideality factor must still be known to calculate the dynamic resistance of the junction and extract an accurate estimate for the series resistance. In [91], the series resistance is extracted using a combination of AC signal measurements and separately calculated value for the thermal resistance.

In principle, pulsed measurements can be used to extract the I-V parameters so rapidly that the diode under test has no time to react thermally. However, if the device under test (DUT) is a Schottky diode with a thermal time constant less than 100 ns, the pulsed system should provide synchronized source-and-measure capability for pulse lengths in

the order of a few tens of nanoseconds. This requires a complicated test setup with dedicated equipment, careful probe selection, and accurate calibration of the cables and interconnects. To the author's knowledge, successful pulsed determination of the series resistance has not been reported for submicron anode Schottky diodes.

The thermal resistance can be determined from simulations [97] or from measurements. The general idea in the measurement-based determination of the thermal resistance of a Schottky diode (also applicable to other diodes and transistors) is to determine the junction temperature and then, with the knowledge of the ambient temperature and power dissipated in the junction, the thermal resistance can be calculated using (4.7). The measurement-based methods include pulsed excitation of the diodes [92], [98], [99], methods based on electrical junction temperature measurements [100], and imaging methods [101]. To the author's knowledge, such successful measurement have not been reported for submicron anode Schottky diodes.

Paper [V] and Section 4.4.4 present a method for simultaneous extraction of the series resistance and thermal resistance of a Schottky diode.

4.4.2 C-V Parameter Extraction

The total capacitance of a Schottky diode can be roughly divided into junction capacitance and parasitic capacitance. Using the junction capacitance definition in (4.11), the total capacitance can be expressed as

$$C_T = C_j + C_p = \frac{C_{j0}}{\left[1 - V_b / \Phi_{bi}\right]^{\frac{1}{2}}} + C_p \, . \tag{4.15}$$

In the case of non-uniform doping of the epilayer, the exponent is not exactly 0.5. However, for the resistive mixer diodes, such as those used in this work, this is a reasonable assumption.

Several methods have been proposed for determining junction and parasitic capacitances (and built-in voltage) of a Schottky diode. These include the use of theoretical calculations [102], physical simulations [103], full-wave electromagnetic

modeling [69], [104]-[106], low-frequency measurements with an impedance analyzer [107] or with an LCR meter [93], [108], [109], and extraction from microwave measurements [95], [110].

Measurement-based determination of the C-V parameters starts with the measurement or extraction (e.g., from S-parameters) of the total capacitance of the diode as a function of the applied voltage. The C-V parameters are then extracted by fitting (4.15) to these values in the least-squares sense. This is illustrated in Figure 23, where C_T values of an SC2T6 diode are obtained by extracting them from low-frequency S-parameters as explained in [VI]. Paper [VI] and Section 4.4.5 present a quantitative comparison and assessment of the capacitance determination techniques using low-frequency LCR meter measurements and microwave frequency S-parameter measurements.

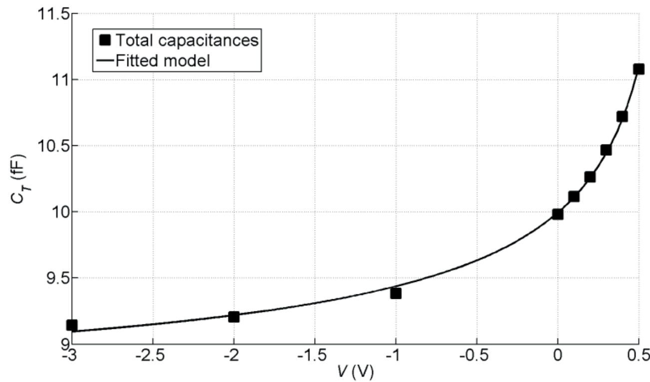

Figure 23. C-V extraction. Equation (4.15) is fitted to total capacitance values extracted from S-parameter measurements. The data is for an SC2T6 diode.

4.4.3 S-parameter Measurement and Characterization

Scattering parameter measurements can be used to verify the results obtained using the I-V and C-V extraction methods described above. In addition, it is also possible to extract the finger inductance of the diode. The S-parameter measurement also reveals whether the circuit environment in which the diode is mounted exhibits unusual behavior. For example, too thick a substrate enables the coupling of surface wave

modes to the wanted propagation mode and ungrounded CPW ground planes might act as a microstrip antennas, destroying the performance of the circuit [111]-[113].

As an example, the measured S-parameters and simulated S-parameters of the equivalent circuit in Figure 16 are shown in Figure 24. It can be seen from the figure, that the equivalent circuit model describes the behavior of the diode well, except for the small amplitude deviation above 95 GHz (at 110 GHz ΔS_{21} = 0.8 dB). The extracted parameters and the calculated cutoff frequencies of the discrete diodes are given in Table 1.

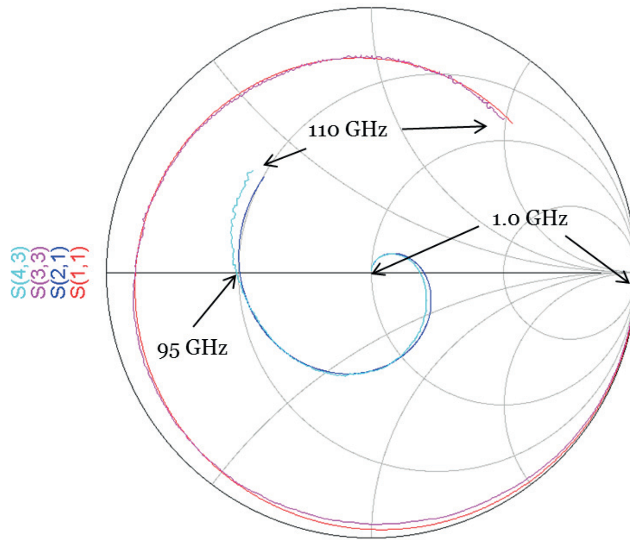

Figure 24. S-parameter measurement and simulation result for an SC2T6 diode using equivalent circuit in Figure 16 at 1 – 110 GHz. Diode is not biased (0 V). S(1,1) and S(2,1) are the reflection and transmission coefficients from the equivalent circuit simulation. S(3,3) and S(4,3) are measured reflection and transmission coefficients.

Table 1. Extracted I-V and C-V parameters, finger inductance and calculated cutoff frequency of an SC2T6 and a 1MSQ08 diode. The series resistance is extracted at 5 mA bias point.

Parameter	SC2T6	1MSQ08
I_S (fA)	0.10	0.15
η	1.24	1.27
R_S (Ω)	4.5	5.9
C_{jo} (fF)	1.81	1.29
C_p (fF)	8.55	5.58
Φ_{bi} (V)	0.77	0.97
L_{ind} (pH)	42	42
f_c (THz)	19.5	20.9

4.4.4 Schottky Diode Series and Thermal Resistance Extraction

This section presents a novel method for the simultaneous extraction of the series resistance and thermal resistance of a Schottky diode. The method, necessary measurements, and the obtained results are discussed in detail in [V]. The full description of the method is laborious and is therefore only summarized here.

The new method combines two different approaches for the extraction of the series resistance of a Schottky diode. As a result, a system of two independent equations is formed, containing two unknowns, the thermal resistance and the series resistance, both of which can then be solved numerically. The approaches are described here as

a) Series resistance extraction from temperature controlled I-V measurements

b) Series resistance extraction from S-parameter measurements

a) The assumption of a constant saturation current and ideality factor leads to too small a value for the extracted series resistance as illustrated in Figure 22. The temperature dependence of the junction can be taken into account by substituting (4.5) and (4.6) into (4.4) and then substituting (4.7) for the junction temperature. The series resistance could now be calculated at all I-V points, if the junction temperature (or thermal resistance) is known. The formula for the series resistance is

$$R_S = \frac{\Delta V_{error} + \Delta V}{I} = \frac{V}{I} - \frac{\eta[T_J(R_\theta)]kT_J(R_\theta)}{qI}\ln\left(\frac{I}{I_S[T_J(R_\theta)]}\right). \quad (4.16)$$

The temperature dependent models for the saturation current and ideality factor are extracted from temperature-controlled I-V measurements and in the current range, where the self-heating has negligible effect. The extracted values and the fitted model for an SC2T6 diode are shown in Figure 25. It can be seen that the temperature dependence can be well modeled using (4.5) and (4.6).

b) On the other hand, the dynamic resistance of a Schottky diode can be extracted using an AC signal. The dynamic resistance contains the resistance of the junction and the series resistance.

$$r_T = \frac{\eta(T_J)kT_J}{qI} + R_S \Rightarrow R_S = r_T - \frac{\eta[T_J(R_\theta)]kT_J(R_\theta)}{qI}. \quad (4.17)$$

In order to obtain reliable, accurate results, the AC signal power and frequency must be carefully selected, as explained in [V].

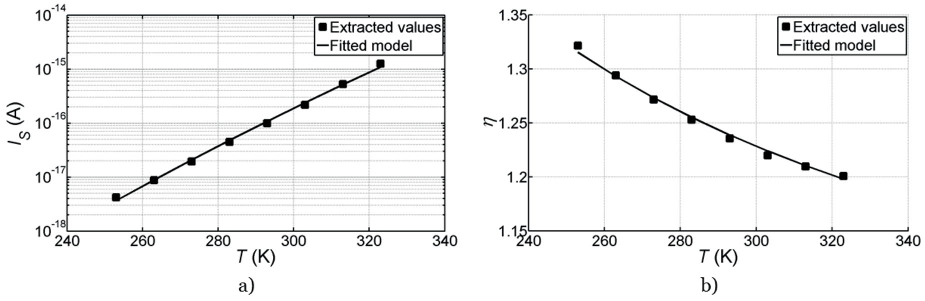

Figure 25. Temperature dependent saturation current and ideality factor of an SC2T6 diode.

The two independent approaches, a) and b), both result in an equation for the series resistance, where the only unknown is the junction temperature (or thermal resistance, depending on whether (4.7) is substituted before solving the system of equations). By eliminating R_S, the junction temperature (thermal resistance) can be solved numerically from

$$\frac{V}{I} - \frac{\eta[T_J(R_\theta)]kT_J(R_\theta)}{qI}\ln\left(\frac{I}{I_S[T_J(R_\theta)]}\right) = r_T - \frac{\eta[T_J(R_\theta)]kT_J(R_\theta)}{qI}. \quad (4.18)$$

After solving the thermal resistance, the series resistance is calculated by substituting the solved thermal resistance back to (4.17). Also (4.16) could be used, but it is more sensitive to a possible error in the extracted value of the thermal resistance, as shown in [V].

When the temperature dependence is taken into account, the extracted values for the series resistance are significantly larger than those obtained using traditional extraction methods. This is illustrated in Figure 26, where results from the traditional extraction are shown together with the results from the new method. The calculated $R_{\theta,ave}$ is the average of the thermal resistance calculated at 1 mA and 5 mA bias points. Results from the new extraction method for an SC2T6 and a 1MSQ08 diode are summarized in Table 2. It can be seen that the series resistance extracted using the new method is significantly larger than that extracted using traditional method. For example, at the 5 mA bias point the difference is 51 % for an SC2T6 diode and 88 % for a 1MSQ08 diode.

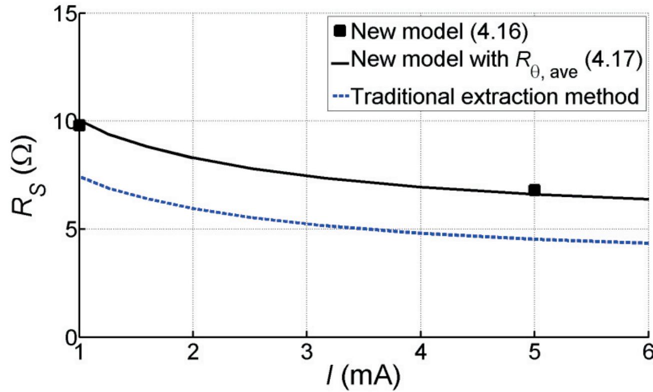

Figure 26. Series resistances extracted using traditional extraction method and the developed new method. Data is for an SC2T6 diode.

The extracted values for the thermal resistance increase with increasing temperature as predicted by [62]. However, the values are somewhat smaller than predicted by (4.9).

This is to be expected, as (4.9) is an approximation for the situation, in which there is no metallization on the diode. In a real diode, the anode finger (good thermal conductor) dissipates part of the heat generated in the junction thus decreasing the thermal resistance. In addition to providing an accurate estimate for the Schottky diode series resistance, the new method is, to the author's knowledge, the only published measurement-based method capable of determining the thermal resistance of Schottky diodes with a submicron anode diameter.

Table 2. Extracted values for the junction temperature, thermal resistance and series resistance of an SC2T6 and a 1MSQ08 diode.

I (mA)	Parameter	SC2T6	1MSQ08
1.0	T_J (K)	298	302
	R_θ (K/W) (1)	4800	9170
	R_θ (K/W) (2)	7890	14050
	R_S (Ω) (1)	9.8	14.1
	R_S (Ω) (3)	7.4	8.4
5.0	T_J (K)	321	348
	R_θ (K/W) (1)	5620	10570
	R_θ (K/W) (2)	8690	16900
	R_S (Ω) (1)	6.8	11.1
	R_S (Ω) (3)	4.5	5.9

(1) Result using the new method

(2) Theoretical value for the thermal resistance

(3) Traditional I-V extraction method

4.4.5 Comparison of Low-Frequency and Microwave Frequency Capacitance Determination Techniques

This section quantitatively compares two capacitance determination techniques, suitable for extracting the C-V parameters of Schottky diodes. The literature review, description of measurement setups, and the different calibration procedures are discussed in Section 4.4.2 and in [VI]. The extraction results and other main findings are summarized here.

The first method is based on the widely-used low-frequency (LCR meter) measurement for determining diode total capacitance. In the second method, the extraction of the total capacitance is done using voltage-controlled S-parameter measurement results.

The diodes are measured as part of a CPW test structure. Test structures are used because the environment, in which the diodes are flip-chip soldered or embedded into the circuit, resembles the situation in which the diodes are used in the usual applications. This is especially true for the discrete diodes, which are usually measured by contacting the pads (open space above the diode). However, when connected to a practical circuit they are usually flip-chip soldered (substrate material below and diode substrate above, Figure 19). The parasitic capacitance of these situations is clearly different.

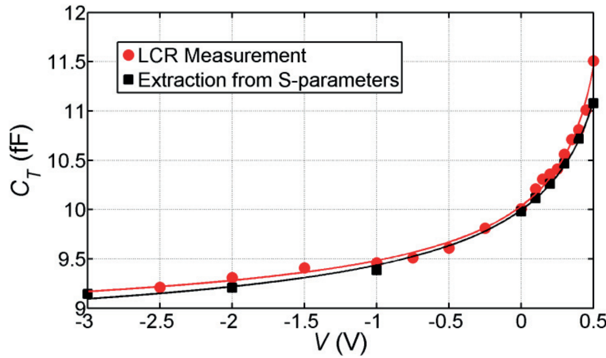

Figure 27. Measured (1 MHz) and extracted (3-10 GHz) total capacitances of an SC2T6 diode. Calibration is performed by measuring an empty test structure.

The measurement results show, that the measured (1 MHz) and extracted (3-10 GHz) total capacitances for discrete SC2T6 diodes match very closely. This is shown in Figure 27. Further, the extracted C-V parameters are in good agreement. The open-ended calibration is performed by measuring an empty test structure and subtracting that capacitance from the measured capacitance of the test structure with a diode. For the 1MSQ08 diode, the comparison could not be performed, as the low-frequency results remained unstable across the frequency and signal amplitude range of the LCR meter. According to the diode manufacturer, this is most likely caused by interface trap states in the AlGaAs membrane substrate.

In the case of MMIC diodes, the low-frequency measurement and extraction from S-parameter results did not yield similar total capacitances. The open-ended calibration by lifting one or both of the whiskers, or by measuring a fabricated test structure without the diode and then subtracting that from the measurement of the test structure with the diode did not result in the same values as those obtained from S-parameter results, as shown in Figure 28. From the extracted C-V parameters C_{jo} and Φ_{bi} are in close agreement, while the parasitic capacitance C_p differs significantly. When the calibration is done by lifting one or both of the whiskers, the extracted parasitic capacitances become much larger than those obtained using S-parameter results. The reason for this is that when the contact is made, a large extra capacitance is introduced by the CPW line center conductors.

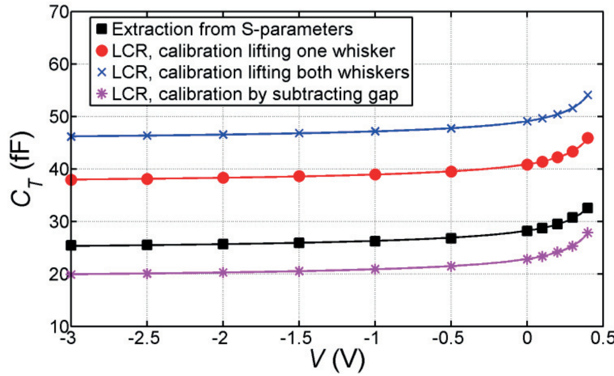

Figure 28. Measured (1 MHz) and extracted (3-10 GHz) total capacitances of a UMS diode with the anode width of 5 μm.

In those cases when the calibration is performed by measuring an empty MMIC test structure, the obtained parasitic capacitance is smaller. The cause of this smaller value in the extracted parasitic capacitance is the significant pad edge-to-pad edge capacitance in MMIC diodes, which is not taken into account when empty test structure is used as a calibration reference. In the case of discrete diodes, this effect is negligible, since the gap between the pad edges is wide and the substrate (fused quartz, ε_r = 3.8) is of much lower permittivity than that of the MMIC diodes (GaAs, ε_r = 12.8). The extracted C-V parameters of an SC2T6 diode and a UMS 5 μm diode are given in Table 3.

To summarize, capacitance extraction from microwave frequency S-parameter measurement results is considered to be a more accurate method for extracting the C-V parameters of discrete and monolithically integrated Schottky diodes for the following reasons

1. In the case of a large pad edge-to-pad edge capacitance the extraction of the C_p (as seen by the RF signal) is difficult from LCR measurements.

2. In the presence of interface trap states, measurement at low frequencies is not reliable.

3. Although not studied in this work, it is well-known that low-frequency signals (basically an alternating electric field) extend far from the actual device being tested and is easily disturbed by the surroundings. In the S-parameter measurement the RF signal is concentrated between the CPW center and the ground plane and is oblivious of its surroundings. This is illustrated in Figure 29.

4. For low-frequency LCR measurements, a larger measurement signal (in this work at least 50 mV) is needed than that for S-parameter measurements with a network analyzer. The reason for this is the very high dynamic range of the network analyzer, which enables accurate measurements using low power levels (in this work always less than -25 dBm). Consequently, using the S-parameters allows capacitances with larger forward voltages to be measured before the diode starts to conduct.

A disadvantage of network analyzer measurement is that it needs test structures with RF probing pads. If large-scale testing is required, as in production testing, low-frequency measurement using needle probe contacts is a feasible option.

Table 3. Extracted C-V parameters of an SC2T6 diode and UMS 5 μm diode. Extraction is performed for the LCR measurement results and for the S-parameter results.

Parameter	$C_{jo}^{(1)}$ (fF)	$C_p^{(1)}$ (fF)	$\Phi_{bi}^{(1)}$ (V)	$C_{jo}^{(2)}$ (fF)	$C_p^{(2)}$ (fF)	$\Phi_{bi}^{(2)}$ (V)
SC2T6	1.5	8.5	0.68	1.6	8.3	0.78
UMS 5 μm	2.2	28.2	0.52	2.2	15.8	0.55

(1) Extracted from LCR meter measurement results, calibration is done by lifting one of the whiskers for UMS diode and by measuring an empty test structure for an SC2T6 diode.

(2) Extracted from S-parameter measurement results.

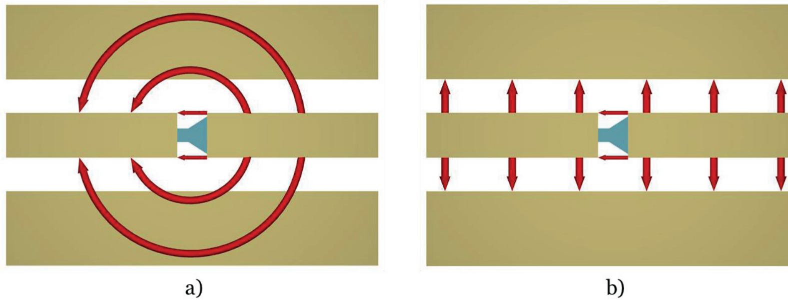

Figure 29. Electric field distribution in a) LCR meter measurement and in b) on-wafer measurement using GSG probes. Note: in a) the field lines do not extend to ground planes, but travel under and above them. Figure only illustrates the electric field distribution.

4.5 Short Summary on Schottky Diode Modeling and Characterization Results

This chapter has briefly introduced the physics behind the operation of the Schottky junction and the consequent I-V and C-V characteristics. Different modeling and characterization methods are discussed and references are given for a comprehensive overview. A novel modeling and characterization method developed in this work is explained, namely, the simultaneous extraction of Schottky diode series resistance and thermal resistance [V]. In addition, this work quantitatively compares low-frequency and microwave frequency capacitance determination techniques [VI].

The new extraction method enables an accurate extraction of the series resistance of the diode, avoiding the inaccuracies in traditional extraction techniques caused by self-heating of the diode. For the two different types of THz Schottky mixer diodes measured in this work, the difference in the values from the traditional extraction and from the new method are 51 % for the diode with an anode radius of 0.7 µm and 88 % for the diode with an anode radius of 0.4 µm. This is a significant difference and has consequences for circuit design. For smaller anodes, this effect is even more pronounced and might be a significant cause for error in the design of a submillimeter-wave mixer or multiplier circuits using Schottky diodes.

This work quantitatively compares capacitance determination techniques at low-frequencies (1 MHz, LCR meter) and at microwave frequencies (3-10 GHz, network analyzer). It is shown that the extraction from S-parameter measurement results offers a more accurate estimate for the parasitic capacitance of a monolithically integrated diode and avoids potential problems in low-frequency measurement caused by interface trap states. In addition, S-parameter measurement can be done at higher bias voltages than is possible with an LCR meter without switching the diode to a conducting state.

5 Applications

Chapters 3 and 4 introduced millimeter wave waveguide impedance tuning devices as well as the Schottky diode measurement and characterization methods used and developed in this work. In this chapter, three applications are presented for utilizing these devices and methods. The applications are relevant to the fields of millimeter wave material characterization, monolithic Schottky diode frequency multipliers, and Schottky mixer diodes used in the waveguide environment.

The intent is not to go through the entire research field in question, but to demonstrate and validate the performance of the waveguide impedance tuning devices and Schottky diode modeling and characterization methods. Nevertheless, each application also contributes to the current state-of-the-art of the related research field. These contributions are highlighted in the discussion and references to the prior art are given.

5.1 Material Measurement at the W-Band Using Multiwaveguide-Band Backshort

Material characterization is a massive field of research. RF signals have been used for decades to evaluate solid materials, liquids, and gases. An excellent description of the different characterization methods used at RF and microwave frequencies is given in [114]. At millimeter wavelengths, the conventional characterization methods are based on measurements in an open resonator, filled waveguides, coated transmission lines [115], or in the free space [116]. To avoid numerical or sample-size related problems, methods are sometimes used that are based on dielectric waveguides [117] or partially filled waveguides [118].

In this section, a method is presented for determining the dielectric constant of solid materials at the W-band [IV]. The method also allows estimation of the loss tangent of the material, though this is not considered to be accurate enough to compete with resonator-based characterization methods. The new method utilizes the multiwaveguide-band backshort presented in [II] and Section 3.1.1. The

characterization is straightforward. The multiwaveguide-band backshort is connected to a waveguide and the dielectric material is inserted into the waveguide at the desired step size (here 0.5 mm and 1.0 mm). This characterization method is illustrated in Figure 30. The reflection coefficient across the W-band is measured at every step and the measured values are matched to the values calculated using the finite-element method (ANSYS HFSS™) when varying the value for the dielectric constant. The dielectric constant giving the best fit with the measurement results is the estimate for the dielectric constant of the material. Precise knowledge of the material slab thickness and width is needed for accurate characterization.

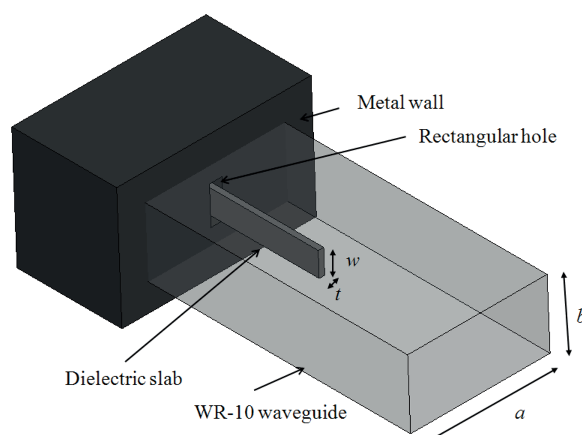

Figure 30. Illustration of the use of the multiwaveguide-band backshort in material characterization.

The method is validated by measuring a well-known material, fused quartz, which has a dielectric constant $\varepsilon_r \approx 3.8$ from RF up to THz frequencies. Results from validation measurements and simulations are shown in Figure 31 a). The agreement in measured and simulated reflection coefficient phase is excellent. After the validation, a slab of unknown glass-like material is attached to the multiwaveguide-band backshort, and the measurement and simulation procedure is repeated. Based on the matching of measured and simulated reflection coefficient phase at different lengths of the dielectric slab inserted into the waveguide, the dielectric constant $\varepsilon_r \approx 7.0$ is determined for a glass-like material. An estimate for the loss tangent of the glass-material is also determined based on the magnitude of the measured and simulated reflection

coefficient. An average loss tangent $\tan\theta = 0.03 \pm 0.005$ is obtained and a slight increase in the loss tangent is also observed as shown in Figure 32.

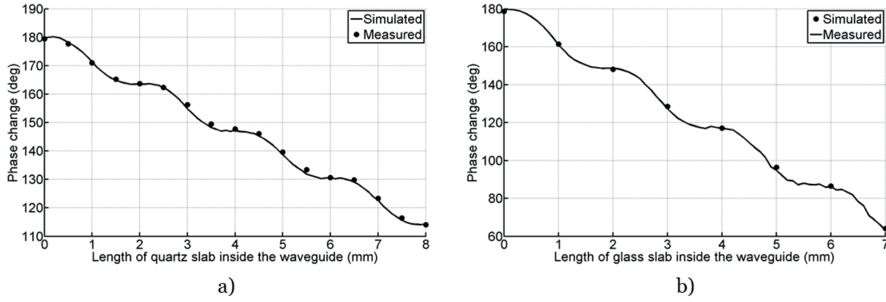

Figure 31. Phase change in the reflection coefficient at 92.5 GHz. In a) dielectric slab is fused quartz and in b) it is glass material.

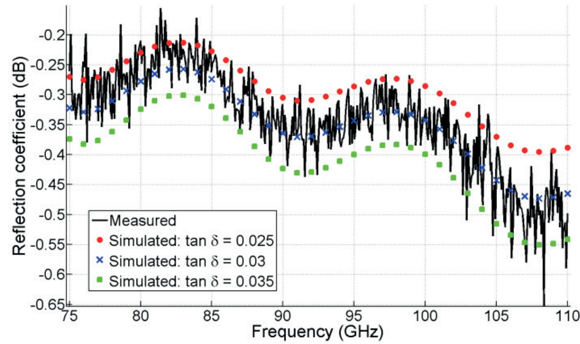

Figure 32. Measured reflection coefficient over the W-band with 7 mm of glass-like material inserted into the waveguide.

The combination of multiwaveguide-band backshort measurement and full-wave simulation is a fast, reliable method for determining the dielectric constant and an estimate of the loss tangent for dielectric materials. Compared to existing material parameter extraction methods, it provides several advantages. First, despite the criticism by the scientific community concerning the simulation approach, finite-element based full-wave simulation provides an accurate tool for determining the S-parameters of well-defined passive structures and is more flexible in terms of geometry and material parameters than most in-house codes. Second, the material

geometry and/or the waveguide need not be fabricated with micrometer precision, as the dielectric material thickness and width are much less than those of the waveguide. Furthermore, the guide channel in the multiwaveguide-band backshort ensures the correct positioning of the slab. The third and most important advantage is that the amount (slab length) of the material in the waveguide can be controlled with micrometer precision. This enables the least-squares fitting of the results at different slab lengths and hence a more accurate estimate for the material parameters. The least-squares fitting also averages out the possible defects or cuts in the material, which could not be detected by measuring only one block of material with known dimensions.

The estimated accuracy for determining the material parameters is ±0.1 for the dielectric constant and ±0.005 for the loss tangent. The limiting factor for the accuracy of the method is the measurement accuracy of the thickness and width of the dielectric material, as well as the stability of the measurement system.

5.2 MMIC Frequency Tripler for 75-140 GHz

Frequency multipliers are needed as signal sources for frequencies above 100 GHz, where fundamental, electrically swept sources are difficult to realize. Some application areas, such as in communication or as an input signal source for higher frequency multiplier, require high output power levels. In order to reach high power levels, multipliers are used that are based on reactive components, like Schottky varactors [119], [120] or heterostructure barrier varactors (HBV) [121].

In applications such as test instrumentation or as the signal source for wideband mm-wave or THz imaging systems, a broad frequency band and output power flatness are often favored at the expense of output power level. High output power and broadband operation are challenging to realize simultaneously, as the reactive components, capable of delivering high power, are difficult to match over broad bandwidth. For this type of applications, it is more suitable to use multipliers based on transistor technology [122], [123] or resistive Schottky diodes [124], [125]. Transistor multipliers can provide good conversion efficiencies and ease of integration with other active

components, such as amplifiers, but cannot handle as large input power and are not as stable as the diode multipliers.

This section presents a compact, broadband MMIC Schottky frequency tripler covering two overlapping frequency bands (W-band, 75-110 GHz and F-band, 90-140 GHz) [VII]. The tripler is optimized to work at low input power levels and offer flat output power across the frequency range. The tripler is fabricated with a UMS BES process and uses monolithic Schottky diodes with anode size of 1x3 μm^2. The diodes are similar to those characterized in [VI].

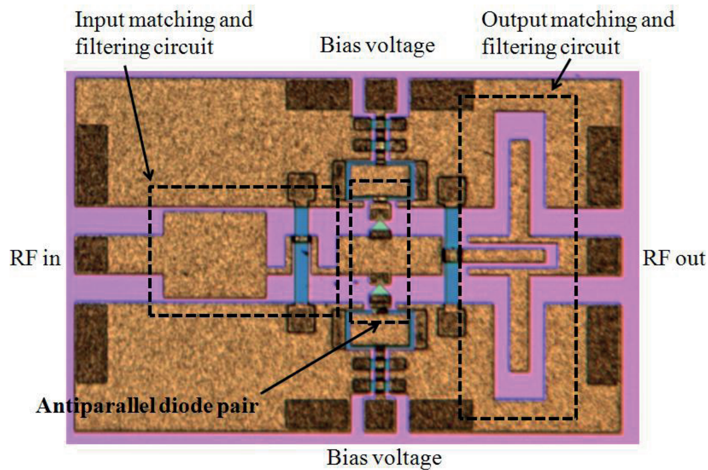

Figure 33. Micrograph of the tripler circuit and the explanation for different parts.

The circuit consists of an input and output matching/filtering circuits and a shunt antiparallel diode pair. A micrograph of the tripler circuit is shown in Figure 33. The tripler is designed by combining full-wave simulator and circuit simulator approaches, as explained in Sections 4.2.3 and 4.2.4. The passive part of the circuit is modeled using ANSYS HFSS™ and the nonlinear part, i.e., the diode junction, is modeled with circuit simulator ADS (circuit model for the junction is shown in the blue rectangle in Figure 16). The input and output matching/filtering circuits are custom designed using a full-wave simulator. This approach makes it possible to develop small circuit components with high performance. The antiparallel diode pair is well-suited for frequency tripler applications, as the even harmonics are trapped in a virtual short circuit created by the diodes and suppressed [58], [126].

The results of the tripler circuit with 2 mW of input power are shown in Figure 34. The maximum output power of -14.7 dBm and efficiency of 1.68 % is measured at 108 GHz. The average efficiency across the output frequency band is 1.1 %. The largest difference in the in-band output power level is 4.7 dB.

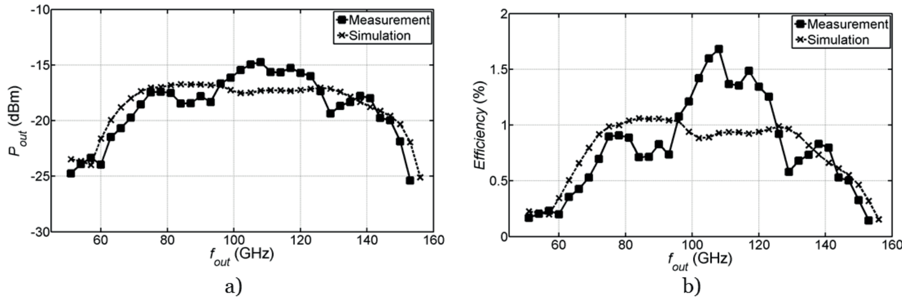

Figure 34. Tripler a) output power and b) efficiency at 75 – 140 GHz with 2 mW of input power. Bias current is kept at a constant value of 2.5 mA during the frequency sweep.

To the author's knowledge, the tripler reported in [VII] is the first solid-state millimeter wave multiplier to cover two overlapping frequency bands offering 60 % operational bandwidth with a flat output power level. In addition, the die area of the tripler (0.47 mm^2) is only one-third that of the designs with comparable performance at the W-band [124], [125].

5.3 Waveguide Mixer Test Jig for 183 GHz

The conventional characterization methods for Schottky diodes include the well-known I-V, C-V, and S-parameter approaches described in Chapter 4. In this section, a complimentary method is introduced for verifying the results obtained from conventional characterization methods and for demonstrating the mixer performance of the diode under test. In short, this method involves measuring the diode in a waveguide mixer, including a flexible RF, LO, and IF impedance tuning and the ability to change the tested diode by changing the substrate on which the diode is soldered [VIII]. The measured mixer results are summarized here. The design guidelines for single anode diode mixers and the mixer theory is discussed in-depth in [63].

The mixer test jig connects the two main fields of research discussed in this thesis: waveguide impedance tuners and Schottky diodes. The test jig itself consists of an *EH*-tuner [III], which in turn includes the multiwaveguide-band backshort [II], for flexible tuning of RF and LO impedances, and of a previously published waveguide-to-suspended microstrip line transition [127]. The diode tested in the jig is an SC2T6 single anode Schottky diode, i.e., the same diode type characterized in [V] and [VI]. A 3D model showing the different parts of the mixer test jig is shown in Figure 35.

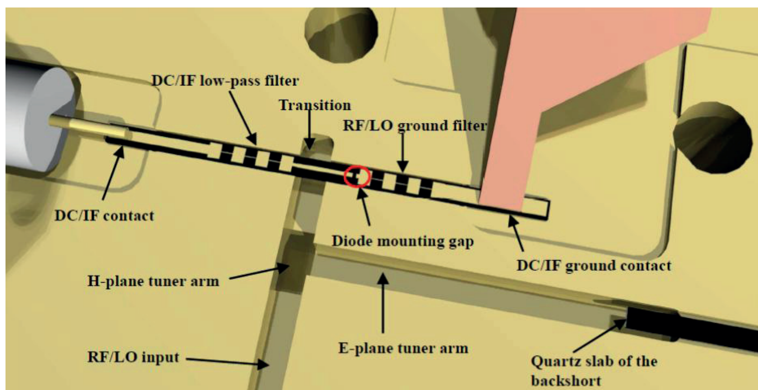

Figure 35. 3D model of the lower split-waveguide block of the test jig.

The setup for mixer double-sideband (DSB) measurements is shown in Figure 36. Conversion loss and noise temperature are extracted using the Y-factor method [128] and the method described in [129]. Single-sideband (SSB) measurements are also performed by using a network analyzer with Oleson V05VNA2-T/R-A extension units for the G-band (140-220 GHz) as the RF source. The results from both measurements are given in Table 4. The effective DSB conversion loss from SSB measurements is calculated using

$$L_{DSB} = \frac{L_S L_i}{L_S + L_i}, \qquad (4.17)$$

where L_S is the conversion loss at the signal frequency, and L_i the conversion loss at the image frequency. It should be noted that the accuracy of the double-sideband measurements is decreased because of the frequency stability and noise of the

backward wave oscillator (BWO) used as the LO source. A solid-state source with sufficient output power was not available at the time of the measurements.

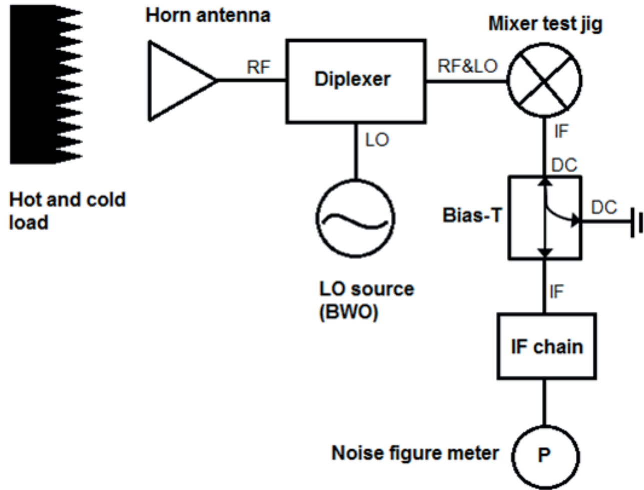

Figure 36. Test setup for DSB conversion loss and noise temperature measurement.

Table 4. Mixer measurement results.

	L_S(1) (dB)	L_i(1) (dB)	L_{DSB}(1) (dB)	L_{DSB}(2) (dB)	T_M(2) (K)
Without IF tuning	7.5	8.5	5.0	4.9	780
With IF tuning	6.5	7.7	4.1	4.6	650

(1) Measured SSB conversion losses using PNA as RF source. L_{DSB}(1) is calculated value from SSB measurements at signal and image bands.

(2) Results are obtained by using the Y-factor method.

In order to compare the performance of the mixer test jig against the predicted mixer performance using the diode parameters extracted in [V] and [VI], a full 3D model of the mixer and diode is constructed in a full-wave simulator, ANSYS HFSS™. The model is shown in Figure 37, and the simulated and measured SSB conversion loss as a function of the LO power in Figure 38. The simulations are carried out using the series resistance values at 5 mA bias point from traditional extraction and from the new

method developed in this work. The diode parameter values are given in [V] and in Table 2. It can be seen from the results that the predicted conversion loss differs within 1.0 dB from the measured one, and that by taking into account the temperature dependent inaccuracy in the series resistance extraction, the difference can be further reduced to less than 0.7 dB. As the difference in the extracted values for the series resistance increases with decreasing diode size, this effect will be more pronounced at higher frequencies, where submicron anode diameters are commonly used in mixer diodes.

The mixer test jig offers an efficient method for testing single anode mixer diodes in their conventional operating environment. Fixed-tuned matching and filtering circuits, which are usually custom-designed to include the effect of the diode geometry, are not needed, as the *EH*-tuner provides flexible matching for RF and LO impedances and coaxial stub-tuner for IF impedance. In addition to diode testing, the test jig can obviously be used as a sensitive stand-alone mixer. As such, it offers conversion loss comparable to the state-of-the-art (L_{DSB} ≈ 4-5 dB) and mixer noise temperature slightly higher than that of the best fixed tuner mixers (T_M ≈ 400-500 K) [130], [131].

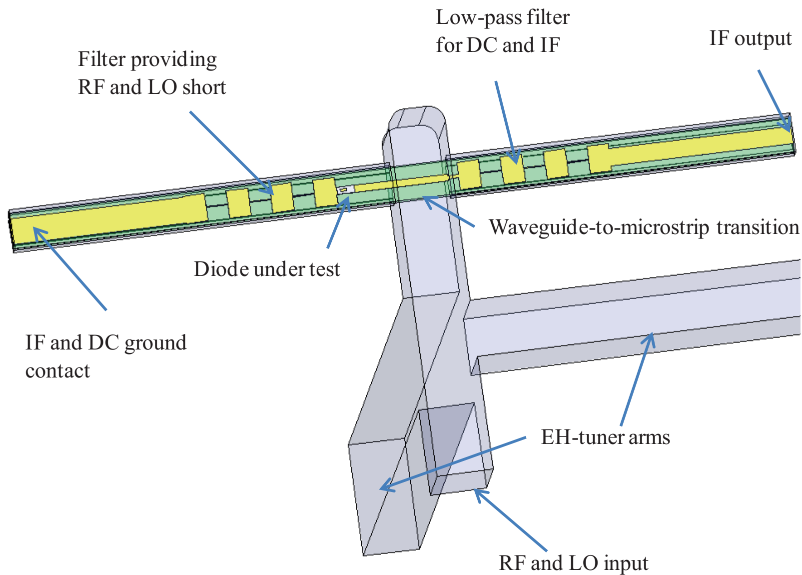

Figure 37. HFSS model of the mixer test jig.

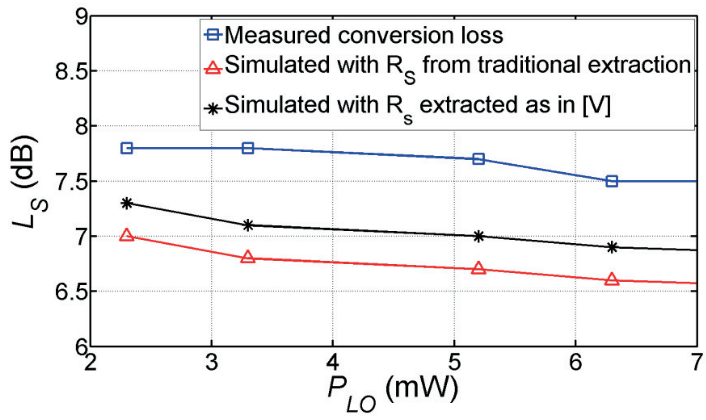

Figure 38. Measured and simulated single-sideband conversion loss of the mixer test jig with an SC2T6 diode.

6 Conclusions and Future Work

The research for this doctoral thesis is related to the fields of millimeter wave waveguide impedance tuners, millimeter wave and THz Schottky diodes, as well as their applications. The results are published in [I]-[VIII]. In this compendium, an effort has been made to introduce the physical operating principles of the studied devices and components and to place the work in an appropriate scientific context.

The work done in this thesis focuses on the design and testing of three millimeter wave waveguide impedance tuners, namely, a double-stub *E*-plane tuner for the W-band [I], multiwaveguide-band backshort [II], and an *EH*-tuner for the G-band [III]. The impedance tuning devices are based on the dielectric backshort concept, and offer advantages over traditional waveguide impedance tuners. These include low losses, no resonance behavior from the backshort unit, high-resolution tuning and the ability to integrate other waveguide components, such as microstrip line transitions, in close proximity of the tuner.

For example, the measured maximum reflection coefficient for the multiwaveguide-band backshort, is larger than 0.972 ($VSWR > 70$) at the center frequencies of the D- and G-band (140 GHz and 180 GHz), and larger than 0.988 ($VSWR > 165$) at the center frequency of the W-band (92 GHz) for any length of the quartz slab between 0 - 8 mm. In addition, the designs presented in [I]-[III] can be straightforwardly scaled to higher frequencies because a “snug” fit or micrometer precision in dimensions of the backshort parts is not necessary for correct operation of the dielectric-based backshort, as it is for traditional waveguide backshorts.

The presented modeling and characterization methods for Schottky diodes include a novel method for simultaneously extracting the series resistance and thermal resistance of a Schottky diode [V], as well as for quantitatively comparing low-frequency and microwave frequency capacitance determination techniques [VI]. The novel extraction method avoids the inaccuracies caused by self-heating of the diode, which are a major concern in traditional I-V extraction methods when the tested diode has a submicron anode diameter. For the two different types of THz Schottky mixer diodes measured in this work, the difference in the values obtained from the traditional extraction

techniques and from the new method are 51 % for the diode with an anode radius of 0.7 μm and 88 % for the diode with an anode radius of 0.4 μm. In addition, this method is, to the author's knowledge, the only published measurement-based method for extracting the thermal resistance of submicron anode Schottky diodes.

Comparison of the capacitance determination techniques demonstrates the advantages and drawbacks of both, low-frequency and microwave frequency determination techniques. It is shown that in many cases, for example, in the determination of the parasitic capacitance of a monolithic diode or in the presence of interface trap states, the extraction of C-V parameters using microwave frequency S-parameter results provides a more reliable method than measurement at low-frequencies.

Three applications are presented, demonstrating the usability of the developed waveguide impedance tuners and/or Schottky diode modeling and characterization methods. The applications relate to millimeter wave material characterization [IV], monolithic Schottky frequency multipliers [VII], and mixer diodes used in the waveguide environment [VIII].

In [IV], the multiwaveguide-band backshort previously presented in [II] is used to extract the permittivity and loss tangent of solid materials at the W-band. The Schottky frequency tripler in [VII] uses monolithically integrated diodes characterized in [VI] and offers 60 % operational bandwidth at 75-140 GHz. The waveguide mixer test jig for single-anode Schottky diodes pulls together the research topics of this work. The test jig uses the *EH*-tuner [III] with the multiwaveguide-band backshort [II] for RF and LO impedance tuning, and the diode type measured and evaluated using the test jig is the same as that characterized and modeled in [V] and [VI]. The test jig offers a double-sideband conversion loss of 4.6 dB and a mixer noise temperature of 650 K.

Future research on the topics discussed in this thesis could involve the scaling of the multiwaveguide-band backshort and possibly the *EH*-tuner for submillimeter wave- and THz frequencies, as well as material parameter extraction in the frequency range of 75-750 GHz using the developed technique and some older techniques, utilized for the first time at THz frequencies. Another direction for future research is to further develop the thermal resistance extraction method to include the image-force lowering effect and

comparing the developed method against thermal simulation results. A new design for the waveguide mixer test jig is already under development. This new test jig will differ from the test jig presented in [VIII] in that it will have the ability to test antiparallel diode pairs. In addition, the LO signal frequency is approximately half of the RF frequency and, consequently, the LO power can be generated with a low-noise source, such as a Gunn oscillator.

References

[1] J. C. Wiltse, “History of millimeter and submillimeter waves,” *IEEE Trans. Microw. Theory Tech.*, vol. 32, no. 9, pp. 1118-1127, Sept. 1984.

[2] H. H. Meinel, “Commercial applications of millimeterwaves history, present status and future trends,” *IEEE Trans. Microw. Theory Tech.*, vol. 43, no. 7, pp. 1639-1653, July 1995.

[3] P. Siegel, “Terahertz technology,” *IEEE Trans. Microw. Theory Tech.*, vol. 50, no. 3, pp. 910-928, March 2002.

[4] Naval Air Warfare Center, *Electronic Warfare and Radar Systems Engineering Handbook*, Avionics Department AIR-4.5 Washington, DC , USA, 20361, 1999, 5-1.1.

[5] D. M. Pozar, *Microwave Engineering*, John Wiley & Sons, Inc., Hoboken, NJ, USA, 2005, pp. 222 - 264.

[6] V. Zhurbenko, *Passive Microwave Components and Antennas*, Intech Open Access Book, April 2010, Chapter 14.

[7] M. Heimlich, “Get on the same nonlinear page,” *IEEE Microwave Magazine*, vol. 12, no. 2, pp. 32-37, April 2011.

[8] web address: www.ansoft.com/products/hf/hfss/ (4th Nov. 2011).

[9] web address: www.agilent.com/find/eesof-ads (4th Nov. 2011).

[10] web address: http://www.mathworks.com/products/matlab/ (4th Nov. 2011).

[11] M. A. Rothman, “A calibrated tuner for millimeter device evaluation,” in *Proc. Southeastcon '89, Energy and Information Technologies in the Southeast*, Columbia, SC, USA, April 1989, pp. 163–167.

[12] P. G. Huggard, B. N. Ellison, B. Alderman, J. E. J. Warner, B. P. Moyna, D. N. Matheson, T. Nagatsuma, and H. Ito, “1.55 μm photomixer sources for mm-wave heterodyne detection and frequency conversion with Schottky diodes” in *LEOS Summer Topical Meetings Digest*, San Diego, CA, USA, July 2005, pp. 105–106.

[13] Q. Xiao, J. L. Hesler, T. W. Crowe, R. M. Weikle II, Y. Duan, B. S. Deaver, and C. L. Brown, “High-efficiency heterostructure-barrier-varactor frequency triplers using AlN substrates,” in *IEEE MTT-S Int. Microwave Symp. Dig.*, Long Beach, CA, USA, June 2005, pp. 443-446.

[14] A. V. Räisänen, D. Choudhury, R. J. Dengler, J. E. Oswald, and P. H. Siegel, “A novel split-waveguide mount design for millimeter- and submillimeter-wave frequency multipliers and mixers,” *IEEE Microw. Guided Wave Lett.*, vol. 3, no. 10, pp. 369–371, Oct. 1993.

[15] M. Kantanen, M. Lahdes, T. Vähä-Heikkilä, and J. Tuovinen, “A wideband on-wafer noise parameter measurement system at 50–75 GHz,” *IEEE Trans. Microw. Theory Tech.*, vol. 51, no. 5, pp. 1489–1495, May 2003.

[16] T. Vähä-Heikkilä, M. Lahdes, M. Kantanen, and J. Tuovinen, “On-wafer noise parameter measurements at W-band,” *IEEE Trans. Microw. Theory Tech.*, vol. 51, no. 6, pp. 1621–1628, June 2003.

[17] F. De Groote, J-P. Teyssier, T. Gasseling, O. Jardel, and J. Verspecht, “Introduction to measurements for power transistor characterization,” *IEEE Microwave Magazine*, vol. 9, pp. 70-85, June 2008.

[18] C. Tsironis, “Harmonic rejection load tuner,” U.S. Patent 6297649, 2001.

[19] B. Bogdanovich, M. Ebert, M. Egorov, and V. Kaminsky, “Design of an E-H tuner and an adjustable directional coupler for high-power waveguide systems,” in *Proc. EPAC 2002*, Paris, France, June 2002, pp. 506–508.

[20] R. Vähä-Heikkilä, J. Varis, J. Tuovinen, and G. M. Rebeiz, “W-band RF MEMS double and triple-stub impedance tuner,” in *IEEE MTT-S Int. Microw. Symp. Dig.*, Long Beach, CA, USA, June 2005, pp. 923-926.

[21] J. Papapolymerou, K. L. Lange, C. L. Goldsmith, A. Malczewski, and J. Kleber, “Reconfigurable double-stub tuners using MEMS switches for intelligent RF front-ends,” *IEEE Trans. Microw. Theory Tech.,* vol. 51, no. 1, pp. 271-278, Jan. 2003.

[22] Y. Lu, L. P. B. Katehi, and D. Peroulis, “High-power MEMS varactors and impedance tuners for millimeter-wave applications,” *IEEE Trans. Microw. Theory Tech.*, vol. 53, no.11, pp. 3672-3678, Nov. 2005.

[23] R. E. Collin, *Foundations for Microwave Engineering*, McCraw-Hill Book Company, New York, USA, 1966, pp. 259-262.

[24] R. L. Eisenhart and R. C. Monzello, “A better waveguide short circuit,” in *IEEE MTT-S Int. Microw. Symp. Dig.*, Dallas, TX, USA, June 1982, pp. 360-362.

[25] B. N. Ellison, L. T. Little, C. M. Mann, and D. N. Matheson, “Quality and performance of tunable waveguide backshorts,” *Electron. Lett.*, vol. 27, no. 2, pp. 139-141, Jan. 1991.

[26] R. A. Linke and M. V. Schneider, “Millimeter waveguide shorts,” U.S. Patent 4216450, 1980.

[27] M. K. Brewer and A. V. Räisänen, “Dual-harmonic noncontacting millimeter waveguide backshorts: theory, design, and test,” *IEEE Trans. Microw. Theory Tech.*, vol. 30, no. 5, pp. 708–714, May 1982.

[28] J. Stanec and S. Barker, “A micromachined contacting sliding short for high frequency applications,” in *IEEE MTT-S Int. Microw. Symp. Dig.*, Boston, MA, USA, June 2009, pp. 965-958.

[29] A. R. Kerr, "An adjustable short-circuit for millimeter waveguides," *Electronics Division Internal Report No. 280*, National Radio Astronomy Observatory, July 1988.

[30] "Sliding short eases measurements," (anonymous) *Microwaves*, vol. 9, no. 12, p. 26, Dec. 1970.

[31] J. Collard, "Electrical wave guide provided with tuning pistons," U.S. Patent 2675524, 1949.

[32] T. M. Weller, L. P. B. Katehi, and W. R. McGrath, "Analysis and design of a novel noncontacting waveguide backshort," *IEEE Trans. Microw. Theory Tech.*, vol. 43, no. 5, pp. 1023-1030, May 1995.

[33] W. R. McGrath, T. M. Weller, and L. P. B. Katehi, "A novel noncontacting waveguide backshort for submillimeter wave frequencies," *Int. J. Infrared and Millimeter Waves*, vol. 16, no. 1, pp. 237-256, May 1995.

[34] W. R. McGrath, "Noncontacting waveguide backshort," U.S. Patent 5138289, 1992.

[35] T. Newman and K. T. Ng, "Planar noncontacting short circuits for millimetre-wave and submillimeter-wave applications," *IEEE Microw. Guided Wave Lett.*, vol. 2, no. 10, pp. 412–414, Oct. 1992.

[36] H. Xu, Z. Liu, C. H. Smith III, J. L. Hesler, B. S. Deaver Jr., and R. M. Weikle II, "A non-contacting tunable waveguide backshort for terahertz applications," in *IEEE MTT-S Int. Microw. Symp. Dig.*, San Francisco, CA, USA, June 2006, pp. 1919-1922.

[37] V. S. Möttönen, "*Receiver front-End Circuits and Components for Millimeter and Submillimeter Wavelengths*," Doctor Sci. Technol. thesis, Radio Lab., Helsinki Univ. Technol., Espoo, Finland, 2005.

[38] V. S. Möttönen, P. Piironen, and A. V. Räisänen, "Novel tunable waveguide backshort for millimeter and submillimeter wavelengths," *IEEE Microw. Wireless Compon. Lett.*, vol. 11, no. 9, pp. 370–372, Sept. 2001.

[39] V. S. Möttönen and A. V. Räisänen, "Design of a dielectric-based tunable waveguide backshort," in *Proc. 35th Eur. Microw. Conf.*, Paris, France, Oct. 2005, pp. 589–592.

[40] F. Bue, "Compact automatic impedance adapter in a waveguide," U.S. Patent 7795988, 2010.

[41] G. R. Simpson, R. L. Eisenhart, B. B. Szendrenyi, and R. J. Maury, "Reduced height waveguide tuner for impedance matching," U.S. Patent 5910754, 1999.

[42] R. Drury, R. D. Pollard, and C. M. Snowden, "A 75-110 GHz automated tuner with exceptional range and repeatability," *IEEE Microw. Guided Wave Lett.*, vol. 6, no. 10, pp. 378–379, Oct. 1996.

[43] web address: http://www.maurymw.com/MW_RF/Automated_Tuners.php (4th Nov. 2011).

[44] web address: http://www.custommicrowave.com/ (4th Nov. 2011).

[45] N. Marcuvitz, *Waveguide Handbook*, Peter Peregrinus Ltd., London, UK, 1993.

[46] P. I. Somlo and J. D. Hunter, *Microwave Impedance Measurement*, Peter Peregrinus Ltd., London, UK, 1985.

[47] Z. Shen, C. Look Law, and C. Qian, "Hybrid finite-element-modal-expansion method for matched magic T-junction," *IEEE Trans. Magnetics*, vol. 38, no. 2, pp. 385-388, March 2002.

[48] F. Braun, "Über die Stromleitung durch Schwefelmetalle," *Ann. Phys. Chem.,* vol. 156, pp. 556-563, Nov. 1874.

[49] A. H. Wilson, "The theory of electronic semiconductors," in *Proc. of the Royal Society of London*, vol. 133, pp. 458-491, June 1931.

[50] W. Schottky, "Halbleitertheorie der Sperrschich," *Naturwissenschaften*, vol. 26, p. 843, Dec. 1938.

[51] N. F. Mott, "Note on the contact between a metal and an insulator or semiconductor," in *Proc. of the Cambridge Physical Society*, vol. 34, pp. 568-572, Oct. 1938.

[52] A. M. Cowley and S. M. Sze, "Surface states and barrier height of metal-semiconductor systems," *J. Appl. Phys,* vol. 36, pp. 3212-3220, Oct. 1965.

[53] F. A. Padovani and R. Stratton, "Field and thermionic-field emission in Schottky barriers," *Solid-State Electron.*, vol. 9, pp. 695–707, July 1966.

[54] C. R. Crowell and S. M. Sze, "Current transport in metal-semiconductor barrier," *Solid-State Electron.*, vol. 9, pp. 1035–1048, Oct. 1966.

[55] C. R. Crowell and V. L. Rideout, "Normalized thermionic-field (T-F) emission in metal-semiconductor (Schottky) barriers," *Solid-State Electron.*, vol. 12, pp. 89–105, Feb. 1969.

[56] S. M. Sze and K. K. Ng, *Physics of Semiconductor Devices*, John Wiley & Sons Inc., Hoboken, NJ, USA, 2007.

[57] M. Shur, *GaAs Devices and Circuits*, Plenum Press, New York, NY, USA, 1987.

[58] M. T. Faber, J. Chramiec, and M. E. Adamski, *Microwave and Millimeter-Wave Diode Frequency Multipliers*, Artech House, Norwood, MA, USA, 1995.

[59] M. T. Faber and M. E. Adamski, "Semiconductor m-n-n+ diodes for frequency conversion at millimeter and submillimeter waves," *Kwartalnik Elektroniki I Telekomunikacji*, vol. 41, pp. 203-255, 1995.

[60] S. Montanari, *Fabrication and Characterization of Planar Gunn Diodes for Monolithic Microwave Integrated Circuits*, Doctor's thesis, RWTH Aachen, Aachen, Germany, 2005.

[61] H. Zirath, “High-frequency noise and current-voltage characteristics of mm-wave platinum n-n+ - GaAs Schottky diodes,” *J. Appl. Phys.*, vol. 60, pp. 1399-1407, Aug. 1986.

[62] S. Adachi, *GaAs and Related Materials*, World Scientific Publishing Co., Singapore, 1999.

[63] S. A. Maas, *Microwave Mixers*, Artech House Inc., Norwood, MA, USA, 2002.

[64] S. A. Maas, *Nonlinear Microwave and RF Circuits*, Artech House Inc., Norwood, MA, USA, 2003.

[65] E. L. Kollberg, T. J. Tolmunen, M. A. Frerking, and J. R. East, “Current saturation in submillimeter wave varactors,” *IEEE Trans. Microw. Theory Tech.*, vol. 40, no. 5, pp. 831-838, May 1992.

[66] J. T. Louhi and A. V. Räisänen, “On the modeling and optimization of Schottky varactor frequency multipliers at submillimeter wavelengths,” *IEEE Trans. Microw. Theory Tech.*, vol. 43, no. 4, pp. 922-926, Apr. 1995.

[67] J. Grajal, V. Krozer, E. Gonzalez, F. Maldonado, and J. Gismero, “Modeling and design aspects of millimeter-wave and submillimeter-wave Schottky diode varactor frequency multipliers,” *IEEE Trans. Microw. Theory Tech.*, vol. 48, no. 4, pp. 700-711, Apr. 2000.

[68] J. V. Siles and J. Grajal, “Physics-based design and optimization of Schottky diode frequency multipliers for terahertz applications,” *IEEE Trans. Microw. Theory Tech.*, vol. 58, no. 7, pp. 1933-1942, July 2010.

[69] A. Y. Tang and J. Stake, “Impact of eddy currents and crowding effects on high-frequency losses in planar Schottky diodes,” *IEEE Trans. Electron Dev.*, Accepted for publication.

[70] D. N. Held and A. R. Kerr, “Conversion loss and noise of microwave and millimeter-wave mixers: Part 2 - experiment,” *IEEE Trans. Microw. Theory Tech.*, vol. 26, no. 2, pp. 55-61, Feb. 1978.

[71] J. W. Archer, “Low-noise heterodyne receivers for near-millimeter-wave radio astronomy,” in *Proc. IEEE*, vol. 73, no. 1, Jan. 1985, pp. 109–130.

[72] J. Hessler, *Planar Schottky Diodes in Submillimeter-Wavelength Waveguide Receivers*, Doctor’s thesis, University of Virginia, 1996.

[73] J. Hesler, “Design and analysis of antiparallel Schottky diode mixers,” in *Proc. of 8th Int. Conf. on Terahertz Electronics,* Darmstadt, Germany, Sept. 2000.

[74] A. Maestrini, J. S. Ward, J. J. Gill, H. S. Javadi, E. Schlecht, C. Tripon-Canseliet, G. Chattopadhyay, and I. Mehdi, “A 540-640-GHz high-efficiency four-anode frequency tripler,” *IEEE Trans. Microw. Theory Tech.*, vol. 53, no. 9, pp. 2835-2843, Sept. 2005.

[75] B. Thomas, A. Maestrini, J. J. Gill, C. Lee, R. Lin, I. Mehdi, and P. de Maagt, “A broadband 835-900-GHz fundamental balanced mixer based on monolithic GaAs

membrane Schottky diodes," *IEEE Trans. Microw. Theory Tech.*, vol. 57, no. 7, pp. 1917-1924, July 2010.

[76] web address: www.acst.de (4th Nov. 2011).

[77] web address: www.vadiodes.com (4th Nov. 2011).

[78] web address: www.ums-gaas.com(4th Nov. 2011).

[79] H. Norde, "A modified forward I-V plot for Schottky diodes with high series resistance," *J. Appl. Phys.*, vol. 50, pp. 5052-5053, July 1979.

[80] R. M. Cibils and R. H. Buitrago, "Forward I-V plot for nonideal Schottky diodes with high series resistance," *J. Appl. Phys.*, vol. 58, pp. 1075-1077, July 1985.

[81] K. Sato and Y. Yasumura, "Study of forward I-V plot for Schottky diodes with high series resistance," *J. Appl. Phys.*, vol. 58, pp. 3655-3657, Nov. 1985.

[82] M. Missous and E. H. Rhoderick, "New way of plotting current/voltage characteristics of Schottky diodes," *Electron. Lett.*, vol. 22, no. 6, pp. 477-478, Apr. 1986.

[83] S. K. Cheung and N. W. Cheung, "Extraction of Schottky diode parameters from forward current-voltage characteristics," *J. Appl. Phys.*, vol. 49, pp. 85-87, July 1986.

[84] T. C. Lee, S. Fung, C. D. Beling, and H. L. Au, "A systematic approach to the measurement of ideality factor, series resistance, and barrier height for Schottky diodes," *J. Appl. Phys.*, vol. 72, pp. 4739-4742, Nov. 1992.

[85] D. Gromov and V. Pugachevich, "Modified method for the calculation of real Schottky-diode parameters," *Appl. Phys. A*, vol. 59, pp. 331-333, 1994.

[86] M. Saglam, E. Ayyildiz, A. Gümüs, A. Türüt, H. Efeoglu, and S. Tüzemen, "Series resistance calculation for the metal-insulator-semiconductor Schottky barrier diode," *Appl. Phys. A*, vol. 62, pp. 269-273, 1996.

[87] V.S. Möttönen, J. Mallat, and A.V. Räisänen, "Characterisation of European millimetre-wave planar diodes," in *Proc. 35th Eur. Microw. Conf.*, Amsterdam, The Netherlands, Oct. 2004, pp. 921-924.

[88] A. Y. Tang, Schottky *Diodes for Terahertz Applications*, Master's thesis, Chalmers University of Technology, 2008.

[89] S. Aazou and E. M. Assaid, "Schottky diode parameters extraction using two different methods," in *Proc. Int. Conf. Microelectronics*, Dec. 2009, pp. 240–243.

[90] D. N. Held and A. R. Kerr, "Conversion loss and noise of microwave and millimeter-wave mixers: Part 1 - theory," *IEEE Trans. Microw. Theory Tech.*, vol. 26, no. 2, pp. 49-55, Feb. 1978.

[91] A. R. Kerr, "On thermal effects in diode series resistance measurements," *NASA internal report,* New York, NY, USA, July 1982.

[92] B. Mottet, *Zuverlässigkeitsstudien an Höchstfrequenzbauelementen mit gepulsten Techniken (TLP-Methode)*, Doctor's thesis, Technical Univ. of Darmstadt, Institut für Hochfrequenztechnik, 2004.

[93] C. D. Wang, C. Y. Zhu, G. Y. Zhang, J. Shen, and L. Li, "Accurate electrical characterization of forward AC behavior of real semiconductor diode: giant negative capacitance and nonlinear interfacial layer," *IEEE Trans. Electr. Devices*., vol. 50, no. 4, pp. 1145-1148, Apr. 2003.

[94] P. Hulbert, "Use pulse I-V testing to characterize RF devices," *RF & Microwaves* (website), Online ID # 19531, http://www.mwrf.com/Articles/Index.cfm?ArticleID=19531&pg=1 (9th Aug. 2011).

[95] P. B. Winson and S. D. Pritchett, "On-wafer GaAs Schottky diode characterization using an integrated pulse I-V/pulse S-parameter measurement system", in *Proc. ARFTG Conf.*, Florida, USA, Dec. 1991, pp. 36-43.

[96] C. P. Baylis, II and L. P. Dunleavy, "Performing and analyzing pulsed current–voltage measurements," *High Freq. Electron.*, vol. 3, no. 5, pp. 64–68, May 2004.

[97] A. Y. Tang, E. Schlecht, G. Chattopadhyay, R. Lin, C. Lee, J. Gill, I. Mehdi, and J. Stake, "Steady-state and transient thermal analysis of high-power planar Schottky diodes,". *22nd Int. Symp. on Space Terahertz Techn.*, Tucson, AZ, USA, Apr. 2011, paper 3-1.

[98] J. P. Bridge, "Making thermal resistance measurements without test diodes or thermal stages," *Microwave Journal*., vol. 48, no. 11, pp. 122-129, Nov. 2005.

[99] MIL-STD-750E, "Test method for semiconductor devices," Nov. 2006.

[100] J. W. Sofia, "Fundamentals of thermal resistance measurement," analysis Tech, 1995, web address: http://ssl.xmu.edu.cn/download%5CThermal%5CFundamentals%20of%20Thermal%20Resistance%20Measurement.pdf (4th Nov. 2011).

[101] K. Azar and J. R. Benson, "Liquid crystal imaging for temperature measurement of electronic devices," in *Proc. Semi-therm Symp.*, Ward Hill, MA, USA, Feb. 1991, pp. 23-33.

[102] J-M. Dieudonne, B. Adelseck, K-E. Schmegner, R. Rittmeyer, and A. Colquhoun, "Technology related design of monolithic millimeter-wave Schottky diode mixers," *IEEE Trans. Microw. Theory Tech.*, vol. 40, no. 7, pp. 1466-1474, July 1992.

[103] D. Salameh and D. Linton, "Study of the relation between doping profile and diode CV characteristics," *IEEE Trans. Microw. Theory Tech.*, vol. 47, no. 4, pp. 506-509, Apr. 1999.

[104] J. Zhang, P. V. Piironen, V. S. Möttönen, J. T. Louhi, A. O. Lehto, A. Simon, C-I. Lin, and A. V. Räisänen, "Model of a quasi-vertical planar anti-parallel Schottky diode," *International Conference on Microwave and Millimeter Wave Technology*, China, 1998, pp. 130-133.

[105] J. Zhang, *Diode Modeling and Circuit Design of Microwave and Millimeter-Wave Frequency Multipliers and Mixers*, Doctor Sci. Technol. thesis, Radio Lab., Helsinki Univ. Technol., Espoo, Finland, 1998.

[106] A. Y. Tang, V. Drakinskiy, P. Sobis, J. Vukusic, and J. Stake, "Modeling of GaAs Schottky diodes for terahertz application," *34th International Conference on Infrared, Millimeter, and Terahertz Waves*, Korea, 2009, 2 pages.

[107] N. Tugluoglu, F. Yakuphanoglu, and S. Karadeniz, "Determination of the interface state density of the In/p-Si Schottky diode by conductance and capacitance-frequency characteristics," *Physica B*, vol. 393, is. 1-2, pp. 56-60, April 2007.

[108] H. Xu, G. S. Schoenthal, L. Liu, Q. Xiao, J. L. Hesler, and R. M. Weikle II, "On estimating and canceling parasitic capacitance in submillimeter-wave planar Schottky diodes," *IEEE Microw. Wireless Compon. Lett.*, vol. 19, no. 12, pp. 807–809, Dec. 2009.

[109] IC-CAP Modeling Handbook, "CV characterization," web address: http://edocs.soco.agilent.com/display/iccapmhb/CV+Characterization, (4th Nov. 2011).

[110] M. K. Matters-Kammerer, L. Tripodi, R. van Langevelde, J. Cumana, and R. H. Jansen, "RF Characterization of Schottky diodes in 65-nm CMOS," *IEEE Trans. Electr. Dev.*, vol. 57, no. 5, pp. 1063-1068, May 2003.

[111] M. Riaziat, R. Majidi-Ahy, and I-J. Feng, "Propagation modes and dispersion characteristics of coplanar waveguides," *IEEE Trans. Microw. Theory Tech.*, vol. 38, no. 3, pp. 245-251, March 1990.

[112] M. Tsuji, H. Shigesawa, and A. A. Oliner, "New interesting leakage behavior on coplanar waveguides of finite and infinite widths," *IEEE Trans. Microw. Theory Tech.*, vol. 39, no. 12, pp. 2130-2137, Dec. 1991.

[113] W. H. Haydl, "Resonance phenomena and power loss in conductor-backed coplanar structures," *IEEE Microw. Wireless Compon. Lett.*, vol. 20, no. 12, pp. 514–516, Dec. 2000.

[114] J. Baker Jarvis, M. D. Janezic, B. F. Riddle, R. T. Johnk, P. Kabos, C. L. Holloway, R. G. Geyer, and C. A. Grosvenor, "Measuring the permittivity and permeability of lossy materials: solids, liquids, metals, building materials, and negative-index materials," *NIST Technical Note*, Boulder, CO, USA, Dec. 2004.

[115] T. Zwick, A. Chandrasekhar, C. W. Baks, U. R. Pfeiffer, S. Brebels, and B. P. Gaucher, "Determination of the complex permittivity of packaging materials at millimeter-wave frequencies," *IEEE Trans. Microw. Theory Tech.*, vol. 54, no. 3, pp. 1001-2006, Mar. 2006.

[116] D. Bourreau, A. Peden, and S. Le Maguer, "A quasi-optical free-space measurement setup without time-domain gating for material characterization in the W-band," *IEEE Trans. Microw. Theory Tech.*, vol. 55, no. 6, pp. 2022-2028, Dec. 2006.

[117] Z. Abbas, R. D. Pollard, and R. W. Kelsall ”A rectangular dielectric waveguide technique for determination of permittivity of materials at W-band,” *IEEE Trans. Microw. Theory Tech.*, vol. 46, no. 12, pp. 2011-2015, Dec. 1998.

[118] J. M. Catala-Civera, A. J. Canos, F. L. Penaranda-Foix, and E. de los Rayes Davo, “Accurate determination of the complex permittivity of materials with transmission reflection measurements in partially filled rectangular waveguides,” *IEEE Trans. Microw. Theory Tech.*, vol. 51, no. 1, pp. 16-24, Jan. 2003.

[119] N. R. Erickson, R. P. Smith, S. C. Martin, B. Nakamura, and I. Mehdi, “High efficiency MMIC frequency triplers for millimeter and submillimeter wavelengths,” in *IEEE MTT-S Int. Microwave Symp. Dig.*, Boston, MA, USA, June 2000, pp. 1003-1006.

[120] Y. Lee, J. R. East, and L. P. B. Katehi, “High-efficiency W-band GaAs monolithic frequency multipliers,” *IEEE Trans. Microw. Theory Tech.*, vol. 52, no. 2, pp. 529-535, Feb. 2004.

[121] J. Vukusic, T. Bryllert, T. Arezoo, M. Sadeghi, and J. Stake, “A 0.2-W heterostructure barrier varactor frequency tripler at 113 GHz,” *IEEE Electron Dev. Lett.*, vol. 28, no. 5, pp. 340–342, May 2007.

[122] Y. Campos-Roca, C. Schwörer, A. Leuther, M. Seelmann-Eggebert, and H. Massler, “A D-band frequency doubler MMIC based on a 100-nm metamorphic HEMT technology,” *IEEE Microw. Wireless Compon. Lett.*, vol. 15, no. 7, pp. 466–468, July 2005.

[123] I. Kallfass, A. Tessmann, H. Massler, D. Lopez-Diaz, A. Leuther, M. Schlechtweg, and O. Ambacher, “A 300 GHz active frequency-doubler and integrated resistive mixer MMIC,” in *Proc. 4th Eur. Microw. Int. Circuits Conf.*, Rome, Italy, Sept. 2009, pp. 200-203.

[124] M. Morgan and S. Weinreb, “A full waveguide band MMIC tripler for 75 – 110 GHz,” *IEEE MTT-S Int. Microw. Symp. Dig.*, Phoenix, AZ, USA, May 2001, pp. 103-106.

[125] K-Y. Lin, H. Wang, M. Morgan, T. Gaier, and S. Weinreb, “A W-band GCPW MMIC diode tripler,” in *Proc. 32nd Eur. Microw. Conf.*, Milan, Italy, Sept. 2002, Paper M10_2_KYLin.

[126] K. S. Saini, “Development of frequency multiplier technology for ALMA” *ALMA Memo 337,* 2003.

[127] K. Dahlberg, T. Kiuru, J. Mallat, A.V. Räisänen, and T. Närhi, “Simple waveguide-to-suspended microstrip transition with low-pass filter,” in *Proc. 40th Eur. Microw. Conf*, Sept. 2010, pp. 671-674.

[128] “Noise figure measurement accuracy – the Y-factor method” *Agilent Application Note 57-2*, May 2010.

[129] R. Trambarulo and H. S. Berger, “Conversion loss and noise temperature of mixers from noise measurements,” *IEEE MTT-S Int. Microw. Symp.*, Boston, MA, USA, May 1983, pp. 364-365.

[130] B. Alderman, H. Sanghera, C. Price, B. Thomas, and D. N. Matheson, “Fabrication of Reproducible air-bridged Schottky diodes for use at frequencies near 200 GHz,” *IRMMW - THz*, Cardiff, UK, Sept. 2007, pp. 848-849.

[131] D. Porterfield, J. Hesler, T. Crowe, W. Bishop, and D. Woolard, “Integrated terahertz transmit/receive modules,” in *Proc. 33th Eur. Microw. Conf*, Munich, Germany, Oct. 2003, pp. 1319-1322.

Errata

- In [VI] Table 1 subtext states: "(1) Extracted from LCR meter measurement results, calibration is done by lifting one of the whiskers". This is not correct for the discrete SC2T6 diode. In this case the calibration is done by measuring an empty test structure and subtracting its capacitance from the capacitance of the test structure with a diode. In the text this is explained correctly.

The motivation for this thesis is in the ever increasing frequencies of radio engineering applications. Traditionally, the radio signals in the millimeter wave region (frequencies between 30-300 GHz) have found applications mainly in the realm of atmospheric or space science and in military applications. Today, these high frequencies are becoming a part of our everyday life. They are used in wireless local area networks, automotive radar, point-to-point communication, and in security applications. Development and testing of devices for such applications depend on the availability of high performance test instrumentation for generating, manipulating, and detecting the high frequency signals as well as on the accurate and reliable models for the components that are used in the devices.

Aalto-DD 133/2011

ISBN 978-952-60-4407-1
ISBN 978-952-60-4408-8 (pdf)
ISSN-L 1799-4934
ISSN 1799-4934
ISSN 1799-4942 (pdf)

Aalto University
School of Electrical Engineering
Department of Radio Science and Engineering
www.aalto.fi

BUSINESS +
ECONOMY

ART +
DESIGN +
ARCHITECTURE

SCIENCE +
TECHNOLOGY

CROSSOVER

DOCTORAL
DISSERTATIONS